

# Cytomegalovirus restricts ICOSL expression on antigen presenting cells disabling T cell co-stimulation and contributing to immune evasion

---

Angulo, Guillem; Železnjak, Jelena; Martínez-Vicente, Pablo; Puñet-Ortiz, Joan; Hengel, Hartmut; Messerle, Martin; Oxenius, Annette; Jonjić, Stipan; Krmpotić, Astrid; Engel, Pablo; ...

Source / Izvornik: **eLife**, 2021, 10

Journal article, Accepted version

Rad u časopisu, Završna verzija rukopisa prihvaćena za objavljivanje (postprint)

<https://doi.org/10.7554/eLife.59350>

Permanent link / Trajna poveznica: <https://um.nsk.hr/um:nbn:hr:184:503816>

Rights / Prava: [Attribution-NonCommercial 4.0 International](#)/[Imenovanje-Nekomercijalno 4.0 međunarodna](#)

Download date / Datum preuzimanja: **2024-07-27**



Repository / Repozitorij:

[Repository of the University of Rijeka, Faculty of Medicine - FMRI Repository](#)



1 **Cytomegalovirus restricts ICOSL expression on antigen presenting**  
2 **cells disabling T cell co-stimulation and contributing to immune**  
3 **evasion**

4  
5 Guillem Angulo<sup>1†</sup>, Jelena Zeleznjak<sup>2,3†</sup>, Pablo Martínez-Vicente<sup>1,4</sup>, Joan Puñet-Ortiz<sup>1,4</sup>,  
6 Hartmut Hengel<sup>5,6</sup>, Martin Messerle<sup>7</sup>, Annette Oxenius<sup>8</sup>, Stipan Jonjic<sup>2,3</sup>, Astrid  
7 Krmpotić<sup>3</sup>, Pablo Engel<sup>1,4</sup>, and Ana Angulo<sup>1,4\*</sup>

8  
9 <sup>1</sup>Immunology Unit, Department of Biomedical Sciences, Faculty of Medicine and  
10 Health Sciences, University of Barcelona, Barcelona 08036, Spain

11 <sup>2</sup>Center for Proteomics, Faculty of Medicine, University of Rijeka, Rijeka 51000,  
12 Croatia

13 <sup>3</sup>Department of Histology and Embryology, Faculty of Medicine, University of Rijeka,  
14 Rijeka 51000, Croatia

15 <sup>4</sup>Institut d'Investigacions Biomèdiques August Pi i Sunyer, Barcelona 08036, Spain

16 <sup>5</sup>Institute of Virology, University Medical Center, Albert-Ludwigs-University Freiburg,  
17 79104 Freiburg, Germany

18 <sup>6</sup>Faculty of Medicine, Albert-Ludwigs-University Freiburg, 79104 Freiburg, Germany

19 <sup>7</sup>Institute of Virology, Hannover Medical School, Hannover 30625, Germany

20 <sup>8</sup>Institute of Microbiology, Department of Biology, ETH Zürich, Zürich, Switzerland

21 \*Corresponding author: [aangulo@ub.edu](mailto:aangulo@ub.edu)

22 †These authors contributed equally to this work

23 Short Title: MCMV decreases T-cell activation by downregulating ICOSL expression

24 **Abstract**

25

26 Viral infections are controlled, and very often cleared, by activated T lymphocytes. The  
27 inducible co-stimulator (ICOS) mediates its functions by binding to its ligand ICOSL,  
28 enhancing T-cell activation and optimal germinal center (GC) formation. Here, we show  
29 that ICOSL is heavily downmodulated during infection of antigen presenting cells by  
30 different herpesviruses. We found that, in murine cytomegalovirus (MCMV), the  
31 immunoevasin m138/fcr-1 physically interacts with ICOSL, impeding its maturation  
32 and promoting its lysosomal degradation. This viral protein counteracts T-cell  
33 responses, in an ICOS-dependent manner, and limits virus control during the acute  
34 MCMV infection. Additionally, we report that blockade of ICOSL in MCMV-infected  
35 mice critically regulates the production of MCMV-specific antibodies due to a reduction  
36 of T follicular helper and GC B cells. Altogether, these findings reveal a novel  
37 mechanism evolved by MCMV to counteract adaptive immune surveillance, and  
38 demonstrates a role of the ICOS:ICOSL axis in the host defense against herpesviruses.

## 39 **Introduction**

40

41 A robust host response against viral infections requires the activation of the adaptive  
42 arm of the immune system mediated by T lymphocytes. For effective T-cell activation,  
43 in addition to the antigen-specific signal delivered by the interaction of major  
44 histocompatibility (MHC)-peptide complexes and T-cell receptors (TCR), concerted co-  
45 stimulatory signals are essential. These signals come from a number of co-stimulatory  
46 molecules upon interaction with their cognate ligands, expressed on antigen-presenting  
47 cells (APCs) (Sharpe, 2009; Chen and Flies, 2013). The B7-CD28 family of ligands and  
48 receptors comprises molecules of the Ig superfamily that function as co-signaling  
49 molecules modulating T-cell responses (Sharpe and Freeman, 2002). The best  
50 characterized co-stimulatory pathway between members of this family is exemplified by  
51 the T-cell surface receptor CD28, which binds to the activated APC surface molecules  
52 B7-1 (CD80) and B7-2 (CD86). Another co-stimulatory pathway of this family is the  
53 receptor ICOS (inducible co-stimulator, CD278), primarily expressed on activated T  
54 cells and at very high levels on T follicular helper cells (Tfh), which mediates its  
55 functions by binding to its ligand ICOSL (B7-H2, CD275) (Hutloff et al., 1999;  
56 Yoshinaga et al., 1999). ICOSL is constitutively expressed on APCs, such as dendritic  
57 cells (DCs), macrophages and B cells, and it is strongly up-regulated by inflammatory  
58 stimuli (Aicher et al., 2000; Swallow et al., 1999; Yoshinaga et al., 2000). ICOSL  
59 presents a different expression profile as compared to CD80 and CD86, and it is  
60 induced on non-lymphoid cells, such as endothelial cells or epithelial cells  
61 (Khayyamian et al., 2002; Qian et al., 2006). The ICOS:ICOSL receptor pathway leads  
62 to enhanced T-cell activation, proliferation, and Th2 responses (Riley et al., 2002;  
63 Tesciuba et al., 2001). In contrast to CD28, which is essential for the activation of



64 naïve T cells, ICOS is more relevant for the regulation of activated and effector T cells  
65 (Coyle et al., 2000). In addition, ICOS co-stimulation plays an essential role in T-  
66 dependent antibody responses and germinal center (GC) formation, by inducing IL-21  
67 production and Bcl6 expression, consequently controlling isotype switching, somatic  
68 hypermutation, and the generation of memory B cells and plasma cells (Choi et al.,  
69 2011; Hutloff, 2015; Liu et al., 2015). ICOS has also been shown to be required for  
70 optimal CD8<sup>+</sup> T-cell proliferation and cytokine production during recall responses  
71 (Takahashi et al., 2009; Wallin et al., 2001) and NK cell activation (Ogasawara et al.,  
72 2002). Importantly, although the ICOSL:ICOS axis is a crucial tuner of cell-mediated  
73 immune responses, little is known about its role in viral host defence.

74

75 Throughout the process of pathogen-host coevolution, viruses have devised multiple  
76 strategies to counteract host immunity. In particular, in order to ensure their prolonged  
77 survival in their hosts, persistent viruses need to undermine adaptive immune responses  
78 at different levels. A common theme of these viruses is to interfere with the presentation  
79 of antigenic peptides by MHC molecules to T cells. To this end, several large DNA  
80 viruses, particularly herpesviruses, encode multiple proteins, which usually are not  
81 essential for replication *in vitro*, with the capacity to interfere with the MHC molecules  
82 or additional cellular components involved in antigen presentation pathway (Schuren et  
83 al., 2016). Given the importance of APCs in triggering and maintenance of adaptive  
84 antiviral immune responses, herpesviruses have evolved molecular determinants and  
85 mechanisms to impair their functions (Brinkmann et al., 2015; Gewurz et al., 2007).  
86 Among them, different members of the herpesvirus family have been reported to disrupt  
87 the interaction established by co-signaling molecules in infected APCs and their counter  
88 receptors, in particular by downregulating CD80 and CD86. This is the case for

89 example of the human and murine cytomegaloviruses (HCMV and MCMV,  
90 respectively), which cause the downregulation of these two molecules during their  
91 respective infectious courses (Hertel et al., 2003; Loewendorf et al., 2004; Mintern et  
92 al., 2006; Moutaftsi et al., 2002). However, whether viruses have evolved immune  
93 evasion strategies to counteract the ICOSL:ICOS pathway remains largely unexplored.

94

95 Here we report that ICOSL-mediated co-stimulation contributes to the development of  
96 effective anti-MCMV immune responses. In addition, we demonstrate that ICOSL  
97 constitutes a major target of CMVs and other herpesviruses, which potently  
98 downregulate its expression on the surface of APCs. We show that MCMV uses its  
99 immunoevasin m138/fcr-1 to manipulate this co-signaling molecule, impeding a  
100 correct T-cell activation during acute MCMV infection. These results reveal a new  
101 mechanism of viral immune evasion.

## 102 **Results**

103

### 104 **MCMV infection rapidly induces a potent ICOSL downregulation in APCs**

105 ICOSL is constitutively expressed at high levels on APCs, including DCs and  
106 macrophages, which are cell types that are susceptible to MCMV infection. In order to  
107 evaluate whether MCMV has the capacity to alter cell-surface expression of ICOSL, we  
108 initially mock-infected or infected murine peritoneal macrophages, at a multiplicity of  
109 infection (moi) of 10, with a GFP expressing MCMV (MCMV-GFP). Under these  
110 conditions, around 50% of the cells in the culture were infected. Three days later,  
111 cultures were analyzed by flow cytometry to measure the expression of cell surface  
112 ICOSL. At this time point, as expected, the density of MHC I at the cell surface was  
113 strongly reduced (Figure 1A). Notably, a pronounced downmodulation of ICOSL was  
114 also observed in GFP<sup>+</sup> infected cells as compared with uninfected GFP<sup>-</sup> cells from the  
115 same cultures, or with mock-infected samples (Figure 1A). Indeed, ICOSL levels  
116 decreased to almost undetectable levels, whereas the expression of the adhesion  
117 molecule CD62L, used as a negative control, remained unaffected. We next assessed if  
118 these findings could be extended to primary bone-marrow-derived macrophages (BMM)  
119 and dendritic cells (BMDC). Importantly, while robust expression of ICOSL was  
120 observed on all uninfected (mock or GFP<sup>-</sup>) cells, the surface reduction of this molecule  
121 in MCMV infected BMMs and BMDCs was significant (Figure 1B). Similar results  
122 were also obtained upon infection of the macrophage cell line IC-21, the dendritic cell  
123 line DC2.4, and the endothelial cell line SVEC4-10, although the extent of  
124 downregulation differed between them (Figure 1B), being quite dramatic on the IC-21  
125 and DC2.4 cells, and more subtle in the SVEC4-10. Altogether, these findings

126 demonstrate that MCMV infection causes a consistent and specific downmodulation of  
127 ICOSL from the surface of APCs.

128 We then assessed whether *de novo* viral protein synthesis was required for ICOSL  
129 downregulation. To this end, peritoneal macrophages were infected for 72 h (infection  
130 rates, approximately 90%) with UV-inactivated MCMV, and the results showed no loss  
131 of ICOSL surface expression (Figure 1C), indicating that a productive MCMV infection  
132 was required to alter ICOSL expression. To determine the kinetics of ICOSL  
133 downmodulation, we examined its surface expression levels at different time points  
134 following infection of peritoneal macrophages with MCMV-GFP. As shown in Figure  
135 1D, by 4 hours post infection (hpi) the density of ICOSL at the cell surface was  
136 substantially reduced, and by 6 hpi there was barely any ICOSL at the surface of  
137 infected cells. When a similar kinetics was conducted in BMDC and IC-21 cells, the  
138 downregulation of ICOSL differed with respect to timing, beginning to be evident by 8  
139 hpi and 16 hpi, respectively, with the effect becoming more prominent from that time  
140 point onwards. Thus, we concluded that MCMV encodes one or more proteins to  
141 rapidly lower cell surface levels of ICOSL upon infection of APCs.

142

### 143 **The MCMV m138 gene is responsible for ICOSL downmodulation**

144 In order to find the viral gene/s mediating the observed effects on ICOSL expression,  
145 we screened a panel of GFP-expressing MCMV deletion mutants that lack different  
146 regions of the viral genome, and which covered a large number of genes dispensable for  
147 viral replication in cell culture. The levels of ICOSL were monitored by flow cytometry  
148 three days after infection of IC-21 cells with the different mutants. We found that,  
149 except for the deletion mutant MCMV $\Delta$ m128-138, all MCMV mutants tested resulted  
150 in the marked downmodulation of ICOSL expression (Figure 2A; see as an example

151 results for the MCMV $\Delta$ m1-17 mutant). The viral region deleted in MCMV $\Delta$ m128-138,  
152 expanding from ORF m128 to m138, includes some ORFs with functions still  
153 unassigned and others involved in viral-host interactions, such as the m129/m131  
154 chemokine homolog associated with tropism to macrophages (Fleming et al., 1999;  
155 Stahl et al., 2015), or the m138 protein, originally described as an Fc receptor (Thäle et  
156 al., 1994), and later reported to be also implicated in the reduction of cell surface  
157 expression of the NKG2D ligands H60, MULT-1, and RAE-1 $\epsilon$  (Arapović et al., 2009;  
158 Lenac et al., 2006), and interestingly, of the co-stimulatory molecule CD80 (Mintern et  
159 al., 2006), a member of the B7 family to which also ICOSL belongs. Based on this later  
160 feature of m138 and the fact that the viral protein is expressed early during infection, we  
161 speculated that the gene altering ICOSL expression in MCMV infected cells might be  
162 m138. To directly test the hypothesis, we used an MCMV with a deletion in this gene  
163 (MCMV $\Delta$ m138). As illustrated in Figure 2B, during infection of IC-21 cells with  
164 MCMV $\Delta$ m138, cell surface expression of ICOSL was maintained to levels similar to  
165 mock-infected cells, while the levels of CD84, a molecule targeted by the MCMV m154  
166 protein (Strazic et al., 2020), used as a control markedly decreased. These effects were  
167 not due to a growth defect of the mutant virus in IC-21 cells, as indicated in earlier  
168 studies where comparable multi-step growth kinetics between an MCMV deleted in  
169 m137-m139 and parental MCMV were observed (Cavanaugh et al., 1996). These results  
170 revealed that one gene product, m138, is responsible for the complete downregulation  
171 of ICOSL during MCMV infection.

172 We next asked if m138, in the absence of other viral molecules, was sufficient to  
173 decrease cell surface levels of ICOSL. To this end, we cloned the m138 gene fused at  
174 the C-terminus with the GFP protein and used the resulting recombinant plasmid  
175 (named m138-GFP) or the parental GFP only-expressing plasmid (CTL-GFP) to

176 transiently transfect IC-21 cells. Flow cytometry analysis 24 hours after transfection  
177 showed that cells transfected with the m138-expressing construct (GFP+) exhibited a  
178 significant reduction of ICOSL surface expression compared to the untransfected  
179 control cells from the same cultures or mock-transfected cells (GFP-; Figure 2C, left  
180 panel). In contrast, we could not detect any change in the expression of ICOSL in cells  
181 transfected with the GFP only-expressing plasmid (compare GFP+ and GFP- cells in  
182 Figure 2C, right panel). Therefore, these results indicate that m138 is able to exert its  
183 downmodulatory effects on ICOSL expression without requiring the MCMV infection  
184 context.

185

#### 186 **Localization of m138 during MCMV infection**

187 m138 has been predicted to be a 569-aa type I transmembrane glycoprotein (Thäle et al.,  
188 1994). Due to the lack of an m138 monoclonal antibody (mAb), the cellular localization  
189 of this viral protein during MCMV infection has so far not been directly assessed.  
190 Previous studies relied on cells expressing the m138 protein in isolation, or on the  
191 different capacity displayed by cells infected with MCMV or with an MCMV mutant  
192 lacking the viral protein to bind Ig. Thus, in order to detect m138 in the infection  
193 context, we generated a mAb specific for m138, using 300.19 cells stably transfected  
194 with the m138 protein HA-tagged at the N-terminus (HA-m138) as immunogen. Then,  
195 NIH3T3 cells were infected with MCMV-GFP, and m138 expression was analyzed by  
196 indirect immunofluorescence employing this newly generated mAb. As shown in Figure  
197 3A (panels a-c and g), using permeabilizing conditions, the viral protein was detected in  
198 perinuclear compartments and cytoplasmic “large punctate vesicles” in GFP+ infected  
199 cells. Similar results were obtained in MCMV-GFP infected DC2.4 cells (Figure 3-  
200 figure supplement 1). Therefore, these results were consistent with earlier reports in

201 transfected cells, showing the m138 protein being mainly expressed in intracellular  
202 compartments together with markers of the ER, protein disulfide isomerase-A1 (PDI)  
203 and calnexin, in addition with the lysosomal marker LAMP-1 (Mintern et al., 2006;  
204 Thäle et al., 1994). In contrast, in non-permeabilized infected cells, the mAb against  
205 m138 failed to detect the viral protein at the cell surface (Figure 3A, panels d-f),  
206 whereas it could be recognized at this location in the 300.19 cells stably transfected with  
207 HA-m138 (Figure 3C, left panels). When analyzed by flow cytometry, though, a dim  
208 expression of m138 at the cell surface of infected cells could be observed (Figure 3B).  
209 As expected, the viral protein was also strongly recognized at the plasma membrane of  
210 the transfected cell when assessed by flow cytometry (Figure 3C, right panel). Finally,  
211 to evaluate whether m138 could be found in lysosomes, NIH3T3 cells were infected  
212 with MCMVwt for 24 h and stained with LysoTracker Red DND99, a fluorescent  
213 marker that labels acidic components and is employed to identify lysosomes. Infected  
214 cells were then analyzed by immunofluorescence using the m138 specific mAb under  
215 gently permeabilizing conditions (0.02% saponin) to preserve the LysoTracker staining.  
216 The results, illustrated in Figure 3D (panels c, and d), indicated that m138 colocalized  
217 with lysosomes. Indeed, quantification of the m138/lysosome colocalization, using the  
218 Coloc2 plugin from FIJI/ImageJ program, led to Manders colocalization coefficients of  
219  $M1=0.76$  and  $M2=0.80$ .

220

### 221 **m138 prevents ICOSL molecules from reaching the plasma membrane via** 222 **targeting to lysosomal degradation**

223 We next sought to study the mechanism by which m138 downregulates ICOSL. Since  
224 there are no available antibodies capable to detect murine ICOSL in western blot, we  
225 generated an NIH3T3 stable cell line expressing HA-ICOSL. We confirmed by flow

226 cytometry that upon infection with MCMVwt, or following transient transfection with  
227 the plasmid expressing GFP tagged m138, but not after infection with MCMV $\Delta$ m138,  
228 HA-ICOSL levels specifically declined at the plasma membrane of the stable HA-  
229 ICOSL expressing cell line (Figure 4A and B). NIH3T3 HA-ICOSL cells were then  
230 mock-infected or infected with MCMVwt or MCMV $\Delta$ m138, lysates prepared and  
231 western blots performed to examine total ICOSL protein levels by staining for the HA  
232 tag. As shown in Figure 4C, two ICOSL specific bands, with apparent molecular masses  
233 of ~ 51 and 70 kDa, were detected in the HA-ICOSL stable cell line as compared to  
234 untransfected NIH3T3 cells (compare lanes 1 and 2). Notably, in MCMV infected cell  
235 lysates, the 70 kDa band was drastically reduced (lane 4), whereas it was not  
236 substantially altered after infection with MCMV $\Delta$ m138 (lane 5), suggesting that this  
237 band corresponds to the mature surface form of ICOSL. Indeed, a mild treatment of the  
238 NIH3T3 HA-ICOSL cells with trypsin, which selectively cleaves the ectodomains of  
239 molecules at the cell surface, and therefore resulted in the loss of detection of ICOSL  
240 when assessed by flow cytometry (Figure 4D), led to the disappearance of the 70 kDa  
241 band in the western blot (Figure 4C, lane 3). Further demonstration that the larger  
242 ICOSL species corresponded to the one present at the cell surface was obtained from a  
243 parallel experiment in which we immunoprecipitated lysates from biotinylated HA-  
244 ICOSL transfected cells with the anti-HA mAb (Figure 4E). Thus, m138 was altering  
245 the expression of the mature form of ICOSL that reaches the cell surface. In addition,  
246 we noted, that the 51 kDa band was more abundantly expressed in the infected samples  
247 than in the mock-infected samples (Figure 4C, compare lanes 2 with lanes 4 and 5). The  
248 fact that ICOSL was slightly induced at the cell surface after treatment with UV-  
249 inactivated MCMV (Figure 1C), could indicate that virion components or the process of  
250 viral binding may be causing these effects. Supporting this observation, an analysis of



251 extracts from NIH3T3 HA-ICOSL cells infected with UV-inactivated MCMV indicated  
252 that this was the case, with both the 51 kDa and the 70 kDa bands being considerably  
253 more abundant than in the mock-infected samples (Figure 4F, compare lanes 2 and 4).  
254 Thus, MCMV infection initially induces ICOSL expression and m138 subsequently  
255 leads to the depletion of cell-surface ICOSL, but not of the overall intracellular levels of  
256 this molecule.

257 Taking into account the intracellular localization of m138 and the fact that it targets the  
258 B7 costimulatory molecule CD80 early in the secretory pathway, rerouting it to  
259 lysosomes, we contemplated the possibility that the viral protein was behaving in a  
260 similar way to interfere with ICOSL (Mintern et al., 2006). We addressed this issue by  
261 co-transfecting NIH3T3 cells with the plasmid encoding for HA-ICOSL together with  
262 either the construct expressing m138-GFP or an unrelated GFP protein (CTL-GFP), and  
263 analyzing the levels of ICOSL expression by western blot before and after treatment  
264 with a combination of two lysosomal inhibitors, leupeptin and bafilomycin. Under these  
265 transient transfection conditions, and in contrast to the assays in stably transfected  
266 NIH3T3 HA-ICOSL cells, ICOSL and m138 were simultaneously expressed, without  
267 previous existence of ICOSL at the cell surface. As shown in Figure 5A, in cells co-  
268 transfected with the m138-GFP protein, independently of whether or not the lysosomal  
269 inhibitor treatment was applied, the 70 kDa ICOSL band, corresponding to ICOSL on  
270 the cell surface, was not observed (lanes 4 and 5). In addition, the results also evidenced  
271 that the 51 kDa band, corresponding to intracellular ICOSL, augmented (1.5-fold) after  
272 exposure to leupeptin and bafilomycin (compare lanes 4 and 5). In contrast, in cells  
273 expressing the CTL-GFP protein, both the 51 and 70 kDa bands were present, and the  
274 blockade of the lysosomal pathway did not lead to a substantial alteration (1.1-fold) of  
275 any of the two ICOSL forms (Figure 5A, compare lanes 2 and 3). The presence of the

276 70 kDa mature form of ICOSL when the CTL-GFP was expressed, and its absence upon  
277 expression of m138-GFP under conditions of lysosomal inhibition, pointed out that the  
278 viral protein was targeting ICOSL before reaching the cell surface. We then infected  
279 NIH3T3 HA-ICOSL cells with MCMVwt and examined by confocal fluorescence  
280 microscopy m138 and ICOSL expression. A marked colocalization of ICOSL and the  
281 viral protein in perinuclear compartments and in cytoplasmic punctate structures could  
282 be observed, being more robust after treatment with the lysosomal inhibitors (Figure  
283 5B, panels g and h). Accordingly, the expression signal of ICOSL was also increased  
284 after treatment with leupeptin and bafilomycin (compare panels a and e in Figure 5B).  
285 The results also showed augmented levels of m138 upon exposure to the lysosomal  
286 inhibitors (compare panels b and f), indicating that m138 was getting partially co-  
287 degraded with its target. These observations were confirmed by flow cytometry in  
288 permeabilized NIH3T3 HA-ICOSL MCMV-infected cells, where significant higher  
289 levels of expression of both ICOSL and m138 could be detected after blockade of the  
290 lysosomal pathway (Figure 5C). Collectively, the data suggest that m138 precludes the  
291 maturation of ICOSL by targeting it to lysosomes, explaining how the levels of this co-  
292 signaling molecule are decreased at the cell surface.

293

#### 294 **m138 interacts with ICOSL**

295 We then considered the possibility that m138 might be interacting with ICOSL, as it has  
296 been previously shown for CD80. To this end, we performed coimmunoprecipitation  
297 assays using NIH3T3 cells transiently expressing m138-GFP and HA-ICOSL. Proteins  
298 were pulled down by an anti-HA antibody and analyzed by western blot using an  
299 antibody against GFP. Taking into account the potential capacity of m138 to bind IgG,  
300 an immunoprecipitation was carried out with an anti-human Fc antibody as a control.

301 As illustrated in Figure 5D, the m138 protein was recovered when the  
302 immunoprecipitation was carried out with the anti-HA antibody (lane 2), whereas when  
303 using the antibody against human Fc the viral protein was not detected (lane 1). As  
304 expected, after stripping the western blot and reprobing it with an anti-HA antibody, the  
305 51 kDa specific ICOSL band was only observed in the precipitates obtained from the  
306 anti-HA mAb pull downs. These data suggest that m138, either directly or in an indirect  
307 manner, associates with ICOSL.

308

### 309 **Distinct m138 structural domains are required to downmodulate the two members** 310 **of the B7 family, ICOSL and CD80**

311 The ectodomain of m138 is predicted to be composed by three Ig-like domains (Lenac  
312 et al., 2006; Corrales -Aguilar et al., 2014). Previous work using mutant MCMVs  
313 containing m138 versions defective in either three potential Ig-like domains indicated  
314 different structural requirements in this viral protein for the downregulation of the  
315 NKG2D ligands (Lenac et al., 2006). We investigated if this was also the case for m138  
316 to exert its effects on the two co-stimulatory molecules ICOSL and CD80, since this  
317 could allow us to dissect the impact of the viral protein on the two pathways of T-cell  
318 activation. Thus, we created three different m138-GFP mutants, missing the putative N-  
319 terminal Ig domain (Ig1; m138 $\Delta$ Ig1-GFP), the middle Ig domain (Ig2; m138 $\Delta$ Ig2-GFP),  
320 or both the middle and membrane-proximal (Ig3) Ig domains (m138 $\Delta$ Ig2/3-GFP)  
321 (Figure 6A, schematic representation of these constructs). Each m138-GFP mutant  
322 construct was transiently expressed on NIH3T3 HA-ICOSL cells and surface levels of  
323 ICOSL and CD80 were assessed by flow cytometry and compared to those present in  
324 cells transfected with the m138-GFP control. As shown in Figure 6B, the m138 $\Delta$ Ig1-  
325 GFP protein was incapable to significantly reduce ICOSL or CD80 cell surface levels.

326 In contrast, while CD80 surface density decreased in cells transfected with m138ΔIg2-  
327 GFP and m138ΔIg2/3-GFP, these two m138 mutants did not alter in a substantial  
328 manner ICOSL expression. Therefore, we conclude that the Ig1 domain of m138 is  
329 absolutely required for both ICOSL and CD80 downregulation. However, while the  
330 putative Ig2 and Ig3 domains of m138 need to be preserved for the downregulation of  
331 ICOSL, they are dispensable for m138-mediated decrease of CD80 expression.

332

333 **m138 curtails ICOSL-dependent antigen presentation and subsequent CD8<sup>+</sup> T-cell**  
334 **responses during MCMV infection of APCs**

335 The differential structural requirements of m138 to target CD80 and ICOSL permitted  
336 us to specifically address the functional consequences of the disruption of the  
337 ICOSL:ICOS pathway during the course of the MCMV infection. To this end, we  
338 employed two MCMV mutants containing m138 versions lacking either the Ig2 domain  
339 (MCMVm138ΔIg2), or the Ig2 and Ig3 domains (MCMVm138ΔIg2/Ig3). As it  
340 occurred in transfection assays with the m138 mutant plasmids defective in these Ig  
341 domains, infections with MCMVm138ΔIg2 or MCMVm138ΔIg2/Ig3 led to decreased  
342 cell-surface density of CD80 but not ICOSL (Figure 7A). We then performed an *in vitro*  
343 antigen presentation assay assessing the effect of these two MCMV mutants on the  
344 ability of APCs to induce an ICOSL-dependent CD8<sup>+</sup> T-cell response, in comparison to  
345 that of MCMVwt and MCMVΔm138. We co-cultivated BMDCs infected with the  
346 different viruses with naive CD8<sup>+</sup> T cells from splenocytes derived from T-cell receptor  
347 (TCR)-transgenic mouse line in which 90% of CD8<sup>+</sup> T-cells are specific for MCMV  
348 M38 peptide, and measured the percentage of IFN-γ<sup>+</sup> CD8<sup>+</sup> T cells 6 h later (Figure 7B,  
349 schematic model) (Maxi mice; Torti et al., 2011). Remarkably, as illustrated in Figure  
350 7B, both MCMVm138ΔIg2 and MCMVm138ΔIg2/Ig3-infected BMDCs stimulated

351 significantly stronger IFN- $\gamma$  responses by CD8<sup>+</sup> T cells as compared to the MCMVwt  
352 infected cells. Moreover, the magnitude of the IFN- $\gamma$  induction observed with these two  
353 MCMV mutants, which downregulated CD80 but preserved cell surface levels of  
354 ICOSL intact, almost approached the levels obtained in MCMV $\Delta$ m138-infected  
355 BDMCs. These findings provide evidence for a substantial contribution of the m138  
356 protein in the evasion of the CD8<sup>+</sup> T-cell immune response via manipulation of the  
357 ICOSL:ICOS axis (Figure 7B).

358

### 359 **m138 impairs ICOS-dependent T-cell responses *in vivo* and limits virus control**

360 We then explored the relevance of ICOSL interference by m138 during the acute  
361 MCMV infection. First, we sought to confirm that ICOSL downmodulation by MCMV  
362 was taking place in the *in vivo* context. Adult BALB/c mice were intraperitoneally (i.p.)  
363 infected with 2x10<sup>6</sup> PFU of MCMV-GFP, and 48 h later the levels of ICOSL were  
364 analyzed in peritoneal macrophages by flow cytometry. As shown in Figure 8A, we  
365 observed a significant reduction of ICOSL levels, in parallel to those of MHC I used as  
366 a positive control, on the surface of the GFP<sup>+</sup> MCMV-infected as compared to the  
367 uninfected GFP<sup>-</sup> macrophages. In addition, we directly assessed whether ICOSL was  
368 being specifically downregulated by m138 on peritoneal DCs during the *in vivo*  
369 infection. Thus, BALB/c mice were mock-infected or i.p. infected with 1x10<sup>6</sup> PFU of  
370 MCMVwt or MCMV $\Delta$ m138, and at 6 hpi cell surface levels of ICOSL and CD80 were  
371 determined by flow cytometry on infected peritoneal DCs (positive for the MCMV  
372 protein m04) and compared to those on peritoneal DCs derived from mock-infected  
373 mice. Figure 8B illustrates a marked MCMVwt-induced downmodulation of ICOSL on  
374 peritoneal DCs, and a subsequent significant augmentation of the levels of this molecule  
375 in the absence of m138, on the surface of MCMV $\Delta$ m138-infected peritoneal DCs. In the

376 case of CD80, although the downmodulation caused by MCMVwt was subtle, a clear  
377 increase of CD80 levels was detected on MCMV $\Delta$ m138-infected cells when compared  
378 to both mock-infected and MCMVwt-infected DCs. Therefore, these results confirmed  
379 a role of m138 downmodulating ICOSL and CD80 on primary mouse DCs (Figure 8B).

380 It has been previously described that the MCMV mutant depleted of m138 is attenuated  
381 early after infection in an NK-dependent manner, attributing this phenotype to the  
382 already reported activities of this viral protein downregulating NKG2D ligands (Lenac  
383 et al., 2006). Taking in consideration m138 effects on the two co-stimulatory molecules  
384 CD80 and ICOSL, we sought to assess the contribution of m138 at later times of the  
385 acute infection by comparing the *in vivo* phenotype of MCMVm138 $\Delta$ Ig2 with that of  
386 MCMV $\Delta$ m138 and MCMVwt under conditions that included depletion of NK cells or  
387 combined depletion of NK cells and CD4<sup>+</sup> and CD8<sup>+</sup> T cells. Of note, previous work  
388 with MCMVm138 $\Delta$ Ig2 showed that this mutant virus was capable to downregulate  
389 NKG2D ligands MULT-1 and RAE-1 $\epsilon$ , but not H60 cell surface molecules (Arapović et  
390 al., 2009; Lenac et al., 2006). The information of the effects that MCMVwt and mutants  
391 have on these m138 targeted host molecules on the surface of infected cells is indicated  
392 in part C of Figure 8. C57BL/6 mice were intravenously (i.v.) infected with 2x10<sup>5</sup> PFU  
393 of the different viruses, left untreated or treated with the antibodies to deplete specific  
394 lymphocyte subsets, and viral titers in salivary glands and lungs were quantified 14 days  
395 post infection (dpi) (Figure 8D, schematic representation of the assay). As illustrated in  
396 Figure 8D, in the salivary glands, viral titers of MCMVm138 $\Delta$ Ig2, a mutant which is  
397 unable to downregulate H60 and ICOSL, were lower than those of MCMVwt. In fact,  
398 the MCMVm138 $\Delta$ Ig2 titers in this organ were below the detection limits for all  
399 animals, in a similar way as in MCMV $\Delta$ m138 infected mice. NK cell depletion led to a  
400 substantial increase of both MCMV $\Delta$ m138 and MCMVm138 $\Delta$ Ig2 infection in this

401 organ, but importantly, MCMVm138 $\Delta$ Ig2, which was downmodulating CD80 but not  
402 ICOSL, was still heavily attenuated as compared to MCMVwt under these conditions.  
403 This finding indicated that ICOSL targeting by m138 is important for the virus to  
404 increase its load in salivary glands. Conversely, the downregulation of CD80 by m138  
405 did not seem to play a major role during MCMV replication in this organ. Furthermore,  
406 when besides NK cells, CD4<sup>+</sup> and CD8<sup>+</sup> T cells were depleted, MCMVm138 $\Delta$ Ig2  
407 growth in the salivary glands was completely restored, indicating that m138 via  
408 interference with ICOSL evades T-cell responses. It is important to note that when NK  
409 cells together with CD4<sup>+</sup> and CD8<sup>+</sup> T cells were depleted, MCMV $\Delta$ m138 seemed to be  
410 slightly attenuated. This may suggest that m138 is capable to perform additional  
411 immune evasion activities independent of NK and T cells. Similar results were obtained  
412 when viral titers were evaluated in the lungs of the infected animals, although in this  
413 case the contribution of m138 via ICOSL in the control of the MCMV infection seemed  
414 to be less significant (Figure 8D).

415 MCMV has been reported to induce the accumulation of virus-specific IL10<sup>+</sup> CD4<sup>+</sup> T  
416 cells in an ICOSL-dependent manner in salivary glands (Clement et al., 2016). Thus, we  
417 directly addressed the impact of m138 on the evasion of MCMV-specific CD4<sup>+</sup> T cells  
418 responses in various organs. To this end, we adoptively transferred TCR-transgenic  
419 CD4<sup>+</sup> T cells specific for the M25 protein (M25-II; Mandaric et al., 2012) into C57BL/6  
420 SCID mice, depleted them of NK cells, and one day later infected them with 2x10<sup>5</sup> PFU  
421 of MCMVwt or MCMV $\Delta$ m138 (See schematic model in Figure 8-figure supplement 1).  
422 Seven days after infection, the expansion of CD4<sup>+</sup> T cells was determined in the spleen,  
423 lungs and salivary glands. The data, illustrated in Figure 8-figure supplement 1, show  
424 that the frequencies of CD4<sup>+</sup> T cells increased in the three organs analyzed upon  
425 MCMV infection. Moreover, a role of the viral m138 protein participating in immune

426 evasion of CD4<sup>+</sup> T cells could be observed in spleen and lungs when comparing data  
427 from MCMVwt and MCMVΔm138 infections, although this was not the case in the  
428 salivary glands.

429

430 **The ICOSL:ICOS axis contributes to the generation of MCMV-specific humoral**  
431 **immune responses *in vivo***

432 We also sought to determine the importance of ICOSL-mediated co-stimulation for  
433 mounting MCMV-specific T-dependent antibody responses. We approached this, by  
434 inhibiting ICOSL:ICOS interaction during the acute MCMVΔm138 infection via the  
435 administration of a blocking anti-ICOSL antibody. Groups of BALB/c mice were  
436 infected with 2x10<sup>6</sup> PFU of MCMVΔm138 and treated with or without an anti-ICOSL  
437 mAb, starting one day prior infection. Salivary gland draining lymph nodes and spleens  
438 were extracted in order to analyze by flow cytometry different T and B lymphocyte  
439 subsets, and blood collected, at day 14 post infection. As illustrated in Figure 9A, a  
440 marked decrease of the percentage of Tfh cells in both spleen and lymph nodes was  
441 observed when infected mice were deprived of ICOSL-mediated signals. In addition,  
442 while the percentage of follicular B cells was not substantially altered, or was even  
443 slightly higher, upon ICOSL blockade, GC B cells in lymph nodes were dramatically  
444 reduced. Consistent with these observations, an analysis by immunofluorescence of  
445 splenic sections revealed that GCs were smaller in size in the infected mice that  
446 received anti-ICOSL antibody as compared to mice that did not received it, whereas this  
447 was not the case of the follicles, whose sizes seemed not to be affected by the treatment  
448 (Figure 9B). These results, which are in agreement with the phenotype associated with  
449 ICOS absence, pointed to a disturbed production of MCMV specific antibodies during  
450 the primary infection under conditions of ICOSL blockade. No significant differences in



451 the percentage of other cell subsets such as marginal zone B cells, B1 B cell subsets,  
452 plasma cells, or overall CD4<sup>+</sup> and CD8<sup>+</sup> T cells between the two groups of infected  
453 animals were detected (Figure 9-figure supplement 1). In addition, the blockade of  
454 ICOSL also resulted in an increased percentage of naïve CD4<sup>+</sup> T cells in the spleen and  
455 decreased percentages of memory CD4<sup>+</sup> T cells in spleens and lymph nodes (Figure  
456 9A), an indication that long lasting immune protection to MCMV could be also  
457 impaired in the absence of ICOSL:ICOS signaling.

458 Due to the above results and the implication of ICOS in promoting T-dependent  
459 antibody responses, we assessed by ELISA whether the levels of MCMV-specific  
460 antibodies in the sera of the infected mice were altered after ICOSL blockade. We  
461 observed that mice that received the anti-ICOSL antibody had significantly reduced  
462 levels of total IgG specific for MCMV than those that did not receive it (Figure 10A).  
463 When we evaluated the serum levels of the predominant subclasses of natural  
464 antibodies, a substantial decreased production of MCMV-specific IgG1 and IgG2a and  
465 b was detected in infected animals in which ICOSL was blocked, while no differences  
466 were found in the production of MCMV-specific IgG3 or IgM responses between both  
467 groups (Figure 10A). These results indicated that ICOSL-mediated co-stimulation was  
468 crucial for the development of MCMV-specific IgG1 and IgG2 responses.

469 The observed alterations in the humoral responses prompted us to conduct *in vitro*  
470 neutralization assays of MCMV with the serum of the infected mice. As illustrated in  
471 Figure 10B, sera from mice that received the anti-ICOSL antibody exhibited a  
472 significant lower capacity to neutralize MCMV compared to those that did not received  
473 it. Similar findings were obtained when the neutralization assays were performed in the  
474 presence of complement (Figure 10-figure supplement 1). In conclusion, our findings

475 indicate a prominent role of ICOSL:ICOS interactions in the induction of effective T  
476 and B cell responses during MCMV infection.

477

#### 478 **HCMV reduces cell surface levels of ICOSL on APCs**

479 We then investigated if HCMV has also the capacity to interfere with cell surface  
480 expression of ICOSL in APCs. To this end, human primary monocyte-derived  
481 macrophages were infected with HCMV-GFP (TB40/E strain), and analyzed by flow  
482 cytometry 72 hours after infection. In addition, we tested the viral effects on the THP-1  
483 cell line differentiated by treatment with the protein kinase-C agonist phorbol-12-  
484 myristate-13-acetate (PMA). As shown in Figure 11A, in both cell types, HCMV  
485 infection resulted in a marked reduction in cell surface ICOSL expression compared to  
486 non-infected cells in the same culture or to mock-infected cells. In contrast, cell surface  
487 expression of CD70 remained unaffected, indicating that ICOSL molecules were  
488 specifically targeted in HCMV infected cells. Kinetic assays performed in THP-1 cells  
489 indicated that by 24 hpi ICOSL levels were already drastically reduced (Figure 11B).  
490 As shown in Figure 11C, the fact that upon infection with UV-inactivated HCMV  
491 ICOSL density at the plasma membrane was not significantly different from that of  
492 mock-infected control cells, suggested that the expression of one or more viral gene  
493 products were required to downmodulate ICOSL. We also analyzed whether the total  
494 levels of ICOSL were altered upon infection, by carrying out immunoblot analysis on  
495 uninfected or HCMV infected protein lysates using an anti-ICOSL polyclonal antibody.  
496 As can be seen in Figure 11D, ICOSL in the THP-1 uninfected cells migrated as a broad  
497 band of approximately 70 kDa. In contrast, after infection with HCMV, the levels of  
498 ICOSL were drastically reduced. Interestingly, we observed that treatment with  
499 leupeptin and bafilomycin was not able to significantly restore ICOSL expression.

500

501 **Additional herpesviruses also target cell surface ICOSL**

502 Finally, we asked whether, similar to murine and human CMVs, other human  
503 herpesviruses are also able to alter ICOSL cell-surface expression during the course of  
504 the infection. We focused on HSV-1 and HSV-2, and infected THP-1 cells using GFP  
505 versions of these viruses. Notably, as illustrated in Figure 11E, the levels of ICOSL  
506 were reduced during infection of both HSV-1-GFP and HSV-2-GFP compared to those  
507 of or mock-infected cells. In contrast, surface expression of CD70 did not change,  
508 confirming the specificity of the findings. Moreover, the observation that upon infection  
509 of THP-1 cells with UV-inactivated HSV-1 and HSV-2, only a partial downregulation  
510 of ICOSL was observed, indicated that these two human viruses also harbor genes  
511 targeting ICOSL (Figure 11E). Last, when we evaluated by western blot ICOSL  
512 expression in whole THP-1 cell lysates, a clear reduction of the levels of this molecule  
513 could be appreciated upon infection with both HSV-1 and HSV-2 (Figure 11F).  
514 Altogether, these findings demonstrate that ICOSL downregulation is a strategy used by  
515 different herpesviruses.

## 516 **Discussion**

517

518 Co-stimulatory molecules play a decisive role in shaping the extent and nature of the  
519 cell-mediated adaptive immune response by tuning T-cell activation. Therefore, it is not  
520 surprising that pathogens, including viruses, have devised mechanisms to abrogate their  
521 signaling and blunt host responses that would otherwise limit their replication (Khan et  
522 al., 2012). In this study, we demonstrate that the ligand for the co-stimulatory molecule  
523 ICOS is dramatically diminished from the surface of APCs during infection by different  
524 herpesviruses. With a primary focus on MCMV, the most widely used model to study  
525 CMV infection, we show that the downregulation of ICOSL restricts the magnitude of  
526 MCMV-specific T-cell responses and potentiates viral burden *in vivo*.

527 We describe here that ICOSL expression is slightly induced upon cell exposure to  
528 MCMV, presumably due to viral sensing by pattern recognition receptors. However,  
529 MCMV rapidly removes this molecule from the surface of infected cells by expressing  
530 m138. Infections with an MCMV lacking the *m138* gene, and assays with the viral gene  
531 expressed in isolation, indicate that m138 is necessary and sufficient to decrease ICOSL  
532 cell surface levels. The early-expressed m138 protein, which is an Fc receptor  
533 homologue, has been shown not only to bind the constant Fc domain of IgG, but also to  
534 downmodulate the expression of three cellular ligands of the activating NKG2D  
535 receptor, RAE-1 $\epsilon$ , H60, and MULT-1, and another B7 family molecule, CD80  
536 (Arapović et al., 2009; Lenac et al., 2006; Mintern et al., 2006; Thäle et al., 1994).  
537 Consequently, this viral protein holds the potential to control the antiviral function of  
538 NK and T cells, as well as the humoral response. Hence, the m138 early glycoprotein  
539 provides an excellent example of how CMVs have refined proteins to execute multiple  
540 immune-evasion functions. It is becoming increasingly clear that the evolution of

541 multifunctional proteins is not only a hallmark of RNA viruses, with limited genome  
542 sizes and relatively small number of genes, but that it is also employed by large DNA  
543 viruses to make optimal use of their coding capacity. For instance, MCMV produces the  
544 multifaceted immunomodulatory protein m152, which is capable of downregulating  
545 MHC class I molecules and different RAE-1 isoforms, as well as modulating the cGAS-  
546 STING pathway, thereby evading type I IFN-, NK- and T cell-dependent immune  
547 responses to MCMV infection (Fink et al., 2013; Krmpotić et al., 1999; Lodoen et al.,  
548 2003; Stempel et al., 2019; Ziegler et al., 1997). Moreover, we have recently  
549 demonstrated that by interfering with AP-1 mediated protein sorting, the m154  
550 glycoprotein targets a broad-spectrum of cell surface molecules implicated in the  
551 antiviral NK and T-cell responses (Strazic et al., 2020; Zarama et al., 2014). In HCMV,  
552 this concept is best exemplified by the *US12* family, whose members, as it will be  
553 discussed below, have been reported to alter the expression of numerous plasma  
554 membrane proteins, mainly NK ligands, adhesion proteins and cytokine receptors  
555 (Fielding et al., 2017).

556

557 m138 is a 69 kDa type I transmembrane glycoprotein, largely localized in the ER and  
558 lysosomal compartments, and shown to be further processed into a 105 kDa highly  
559 glycosylated form (Mintern et al., 2006). Based on the ability of MCMV infected cells  
560 to bind IgG, m138 was reported to be a cell surface resident protein, a feature shared by  
561 the different viral Fc $\gamma$  receptors (Corrales-Aguilar et al., 2014; Lenac et al., 2006).  
562 Consistent with its location at the plasma membrane, the viral protein was shown to  
563 perturb the endocytosis of surface RAE-1 $\epsilon$  and MULT-1, interfering with the clathrin  
564 dependent endocytosis of this later cellular target, altering its recycling and leading to  
565 its subsequent degradation in lysosomes (Arapović et al., 2009; Lenac et al., 2006). A

566 different mode of action was reported for m138 in the downregulation of CD80,  
567 targeting the cellular molecule when newly synthesized early in the secretory pathway  
568 and mislocalizing it to lysosomal compartments (Mintern et al., 2006). To date, studies  
569 on the maturation and posttranslational modifications of ICOSL are still lacking, but our  
570 observations are compatible with the notion that, as in the case of CD80, m138 interacts  
571 with ICOSL, preventing it to mature and reach the plasma membrane, and driving this  
572 molecule to lysosomal degradation. Accordingly, we found that during MCMV  
573 infection, m138 and ICOSL colocalize in intracellular compartments, where the viral  
574 protein is primarily expressed, and that upon treatment with lysosomal inhibitors the  
575 levels of both ICOSL and m138 augment. Moreover, our co-precipitation experiments  
576 demonstrate that indeed m138 directly associates with ICOSL. The details on how the  
577 interactions of m138 with its structurally diverse targets can potentially occur remain to  
578 be elucidated. In this regard, solving the crystal structure of m138 alone or bound to its  
579 cellular targets may be of great value for understanding its versatility and different  
580 modes of action.

581

582 Due to the multiple cellular targets of m138, dissecting the functional consequences of  
583 lessening ICOSL cell surface levels on virally infected cells appeared to be complicated.  
584 m138 was predicted to contain an ectodomain with three putative Ig-like domains,  
585 exhibiting a relatively low but yet significant sequence homology with the Ig-like  
586 domains of murine Fc $\gamma$ Rs CD16 and CD32 (Budt et al., 2004; Lenac et al., 2006).  
587 Previous work indicated distinct m138 structural requirements to downmodulate the  
588 different NKG2D ligands (Arapović et al., 2009; Lenac et al., 2006; Mintern et al.,  
589 2006). Thus, by generating versions of the m138 protein devoid of some of its Ig  
590 domains, and through the use of MCMV recombinants bearing similar deletions within

591 the viral protein, we determined that the downregulation of the two B7-molecules,  
592 ICOSL and CD80, was dependent on the N-terminal m138 Ig domain. However, while  
593 the middle and membrane-proximal Ig domains of m138 were largely dispensable for  
594 disturbing CD80, they needed to be preserved for ICOSL cell surface removal. This  
595 result indicates a distinct mode of action of m138 to target the two costimulatory  
596 molecules, and gave us the opportunity to separate the corresponding impacts on T-cell  
597 activation. Optimal T-cell activation is characterized by rapid proliferation, cytokine  
598 production and efficient effector functions. Importantly, employing an *in vitro* antigen  
599 presentation assay and the m138 mutant MCMVs, we showed that via ICOSL  
600 downmodulation, m138 contributes to impair antiviral CD8<sup>+</sup> T-cell responses. This  
601 agrees with the earlier evidence that the m138 protein expressed in isolation is capable  
602 to reduce the ability of DCs to promote T-cell activation in a CD80-dependent manner,  
603 and the fact that applying a blocking anti-CD80 antibody only partially reverted these  
604 effects (Mintern et al., 2006). Our observations, however, in the context of the infection,  
605 point to a prominent role of the ICOSL-dependent m138 function compromising T-cell  
606 stimulation. The m138 protein has not an ortholog in HCMV. However, we demonstrate  
607 that following a productive HCMV infection of primary monocyte-derived  
608 macrophages or differentiated THP-1 cells, which express high levels of ICOSL, a  
609 strong ICOSL cell surface downregulation also takes place, and that this process  
610 requires viral gene expression. Using a multiplexed proteomic approach and HCMVs  
611 with deletions of each individual ORF of the *US12* viral family, Fielding and co-  
612 workers had previously described that members of this family selectively target a  
613 number of plasma membrane proteins crucial for NK cell activity, adhesion, and  
614 cytokine signaling during HCMV infection of human fibroblasts (Fielding et al., 2017).  
615 Interestingly, in these assays, and despite the low levels of ICOSL in human fibroblasts,

616 no reduction of cell surface ICOSL could be observed after infection with HCMVs  
617 deleted in either US16 or US20, strongly suggesting that these two HCMV products are  
618 involved in ICOSL downregulation. Our findings also indicate that HCMV not only  
619 leads to diminished cell surface ICOSL, but also to an abrogation of its expression in  
620 whole cell levels, via a lysosomal degradation-independent process. Importantly, a  
621 similar complete loss of ICOSL on differentiated THP-1 cells was observed during  
622 infection by two  $\alpha$ -herpesviruses, HSV-1 and HSV-2. In this case, though, both the  
623 mechanism as well as the identity of the viral proteins involved in this process remain to  
624 be defined.

625

626 The importance of the ICOSL:ICOS pathway has been explored in several models of  
627 bacterial and parasitic infections (Wikenheiser and Stumhofer, 2016). However, to date,  
628 only a limited number of studies on murine models of infection with RNA viruses  
629 (LCMV, VSV, and influenza virus), in conditions of ICOS deficiency or blockade with  
630 an ICOSL-Ig molecule, have been reported, and shown that ICOS triggering plays a  
631 marginal although significant role in the development of CD4<sup>+</sup> T-cell effector responses  
632 (Bertram et al., 2002; Kopf et al., 2000). But, persisting DNA viruses, with infections  
633 more dependent on cell-mediated immune control, may differ. Besides the role played  
634 by ICOS in directing effector T-cell activation, proliferation and differentiation, this  
635 molecule has been crucially implicated in the generation of T-dependent antibody  
636 responses. Thus, in this study we examined whether anti-MCMV humoral immune  
637 responses were altered in the absence of ICOS signaling. Overall, our data employing a  
638 blocking monoclonal anti-ICOSL antibody in the context of the acute MCMV infection  
639 revealed a high importance of the ICOSL:ICOS axis in the formation of Tfh cells and  
640 subsequent GC B-cell development in spleens and lymph nodes follicles, consistent



641 with what has been previously observed in other *in vivo* experimental models of  
642 infection (Wikenheiser and Stumhofer, 2016). Importantly, as a consequence of the  
643 observed effects, ICOSL blockade was associated with a lower production of MCMV-  
644 specific IgG1 and IgG2 antibodies. Furthermore, a decreased capacity of the antibodies  
645 generated to neutralize MCMV was also observed. Notably, while the  
646 CD80/CD86:CD28 co-stimulatory pathway has been shown to be also involved in the  
647 induction of Tfh cells and class switching of MCMV-specific antibodies, we find that  
648 this pathway is not capable to compensate the defects observed in the absence of ICOS  
649 signaling, evidencing the non-redundant role of the two axis in this scenario (Welten et  
650 al., 2016). We have not directly addressed here whether the lack of ICOSL co-  
651 stimulation is associated with a deficient viral control, due to the highly attenuated  
652 phenotype of the MCMV defective in m138 employed in the study. Remarkably, a  
653 reduction of splenic CD4<sup>+</sup> memory T cells was also observed in our assays upon ICOSL  
654 blockade, further supporting the potential significance of the ICOSL:ICOS axis in the  
655 long term protection against MCMV. Of interest, ICOS- and ICOSL-deficient patients  
656 have been associated with combined T- and B-cell immunodeficiency, and importantly,  
657 with an increased susceptibility to viral infections (Roussel et al., 2019; Schepp et al.,  
658 2017). Moreover, while the infectious phenotype of these patients varied, a high  
659 incidence of recurrent herpesvirus infections, mostly including herpes simplex and  
660 cytomegalovirus infections, was observed.

661

662 It was previously shown that deletion of m138 or both m138 and the CD86  
663 downmodulator m147.5 from MCMV has a dramatic impact on viral load during acute  
664 infection (Arens et al., 2011; Crnković-Mertens et al., 1998). To directly address the  
665 potential importance of m138-mediated downregulation of ICOSL on viral growth *in*

666 *in vivo* we employed the recombinant MCMV expressing m138 without the middle Ig  
667 domain, and therefore able to downmodulate CD80 and CD86 but not ICOSL in  
668 infected APCs. The fact that under conditions of NK cell depletion the viral mutant was  
669 still attenuated at late times post infection, particularly in the salivary glands, and the  
670 nearly complete reversion of this defective phenotype in the absence of NK cells and T  
671 cells, indicated that m138 by interfering with ICOSL contributes to subvert T-cell  
672 responses *in vivo*. By performing adoptive transfer assays of exogenous M25-specific  
673 transgenic CD4<sup>+</sup> T cells into C57BL/6 SCID mice, which were depleted of NK cells,  
674 and infected with MCMVwt or the MCMV lacking m138, we evaluated the impact that  
675 the viral protein may have on immune evasion of CD4<sup>+</sup> T cells in various organs. We  
676 observed that m138 clearly contributes to diminish M25-specific CD4<sup>+</sup> T cell  
677 proliferation in spleen and lungs of infected mice, but not in salivary glands, where  
678 virus specific CD4<sup>+</sup> T cells are important for control of the viral infection. It must be  
679 noted, however, that since in the study we only measured M25-specific responses, we  
680 cannot discard that in the salivary glands m138 may be influencing in a different way  
681 CD4<sup>+</sup> T cell responses specific for other MCMV epitopes. Altogether, our results  
682 support the notion that downmodulation of ICOSL by m138 represents an effective  
683 immune evasion strategy during the acute MCMV infection. Taking in account these  
684 observations, an aspect that deserves to be explored is whether these ICOSL-related  
685 activities can be employed by additional herpesviruses or other viral pathogens as a  
686 mean to escape host immune surveillance.

687

688 In conclusion, in this study we present a novel viral tactic to impair T-cell activation,  
689 based on the interference with the ICOS:ICOSL co-stimulation pathway. To this end,  
690 the herpesviruses analyzed so far seem to exploit “self” proteins, evolved during co-

691 evolution with their hosts, being in the case of murine CMV, a multitasking  
692 immunoevasin. Ultimately, the study of these immunoevasin should provide not only  
693 new insights into viral pathogenesis, but also enlighten us about critical biological and  
694 immunological processes that promote viral control.

695 **Material and methods**

696

697 **Ethics statement**

698 All procedures involving animals and their care were approved (protocol number CEEA  
699 308/12) by the Ethics Committee of the University of Barcelona (Spain) and the Animal  
700 Welfare Committee at the University of Rijeka (Croatia) and were conducted in  
701 compliance with institutional guidelines as well as with national (Generalitat de  
702 Catalunya decree 214/1997, DOGC 2450) and international (Guide for the Care and Use  
703 of Laboratory Animals, National Institutes of Health, 85–23, 1985) laws and policies.  
704 Human blood was obtained from healthy volunteer donors through the Blood and  
705 Tissue Bank of the Catalan Department of Health (Barcelona, Spain). Utilization of  
706 blood products for the experiments conducted was approved by the Ethics Committee of  
707 the Hospital Clinic of Barcelona (Barcelona, Spain), and according to the principles of  
708 the Declaration of Helsinki.

709

710 **Cell cultures**

711 NIH3T3 (mouse embryonic fibroblasts), SVEC4-10 (SV40-transformed mouse  
712 endothelial cells), HFF (human foreskin fibroblasts), HEL299 (human embryonic lung  
713 fibroblasts), MEFs (primary mouse embryonic fibroblasts), MEFs immortalized with  
714 p53 (kindly provided by Dr. Jay Nelson [Oregon Health Sciences University, Portland,  
715 USA]), and Vero cells were cultivated in Dulbecco's modified Eagle's medium  
716 (DMEM) supplemented with 2 mM glutamine, 1 mM sodium pyruvate, 50 U/mL of  
717 penicillin, 50 g/mL of streptomycin, and 10% fetal bovine serum (FBS). IC-21 (mouse  
718 peritoneal macrophages transformed with SV-40), DC2.4 (mouse dendritic), NS1  
719 (mouse myeloma), THP-1 (human monocytic) and 300.19 (mouse pre-B) cells were

720 cultured in RPMI-1640 medium, supplemented as indicated above, and for THP-1 and  
721 300.19 cells, 0.05 mM 2-mercaptoethanol was added. Primary mouse peritoneal  
722 macrophages were elicited from peritoneal exudate cells from BALB/c mice receiving 1  
723 mL of thioglycolate i.p. 4 days before the extraction. Primary peritoneal dendritic cells  
724 were isolated according to Ray and Dittel (2010). Splenocytes and lymph nodes  
725 obtained from mice were subjected to a manual disaggregation and treatment with red  
726 blood cell lysis buffer (0.15 M NH<sub>4</sub>Cl, 0.01 M Tris HCL) to obtain cell suspensions.  
727 Primary mouse dendritic cells and macrophages from bone marrow of femur bones  
728 from BALB/c mice or C57BL/6 were obtained after 7 days of culture in RPMI-1640  
729 medium supplemented as indicated above, with the addition of granulocyte-macrophage  
730 colony-stimulating factor (GM-CSF) at days 3 and 6 from extraction. Attached cells  
731 were enriched in macrophages whereas suspension fractions were enriched in dendritic  
732 cells. Both type of cells were plated in flat-bottom 24-well dishes with the  
733 supplemented RPMI-1640 medium at a concentration of 2x10<sup>5</sup> cells/well. Dendritic and  
734 macrophage differentiation were confirmed by flow cytometry using the markers  
735 CD11c and, F4/80, respectively. Primary human monocytes were obtained from  
736 PBMCs isolated by Ficoll-Paque density-gradient centrifugation from fresh blood  
737 samples of human healthy donors. Monocyte-derived macrophages (MDM) were  
738 differentiated after culturing monocytes for 5 days in RPMI-1640 medium  
739 supplemented as indicated for mouse primary cells, with 50 ng/mL of GM-CSF. Cell  
740 lines were routinely tested for mycoplasma contamination with MycoAlert Mycoplasma  
741 Detection Kit from Lonza.

742

### 743 **Viruses and infections**

744 The bacterial artificial chromosome (BAC)-derived MCMV strain MW97.01, here  
745 referred as MCMVwt (Wagner et al., 1999), and the MCMV-GFP recombinant virus, a  
746 derivative of MW97.01 carrying the GFP gene (Mathys et al., 2003), were used as  
747 parental viruses throughout the study. Recombinant strains MCMV-GFP $\Delta$ 15 lacking  
748 genes from *m128* to *m138* (termed here MCMV-GFP $\Delta$ m128-m138) and MCMV $\Delta$ m138  
749 lacking the *m138* gene, have been described previously (Lenac et al., 2006), as well as  
750 recombinant strain MCMV-GFP $\Delta$ 1 lacking genes from *m1* to *m17* (termed here  
751 MCMV-GFP $\Delta$ m1-m17; Brune et al., 2006). MCMV mutants containing m138 versions  
752 without Ig2 domain (MCMVm138 $\Delta$ Ig2), or without Ig2 and Ig3 domains  
753 (MCMVm138 $\Delta$ Ig2/Ig3) were also described in Lenac et al., 2006. Viral stocks were  
754 grown by infecting MEFs cells at a low moi using DMEM supplemented as stated  
755 above, except that 3% FBS was used. Cell supernatants were recovered when maximum  
756 cytopathic effect was reached, and cleared of cellular debris by centrifugation at 1750 g  
757 for 10 min. The HCMV strain TB40/E carrying the *GFP* gene was used in the study  
758 (termed here HCMV-GFP; Sinzger et al., 2008). HCMV stocks were prepared as  
759 indicated for MCMVs, but using in this case HEL299 or HFF cells. HSV-1 and HSV-2  
760 containing the GFP gene were kindly provided by Dr. Antonio Alcamí (Autonomous  
761 University of Madrid, Spain). Both viruses were grown in Vero cells. Viral titers were  
762 determined by standard plaque assay on primary BALB/c MEFs, MEFs p53, HEL299  
763 or Vero cells for MCMV, HCMV, or HSV-1 and HSV-2, respectively. Infections of  
764 murine peritoneal macrophages, bone marrow dendritic cells and IC-21 cells included a  
765 centrifugal enhancement of infectivity step (Hudson, 1988). C57BL/6 derived DCs were  
766 infected by incubating cells in suspension with the virus for 30 min in a small volume  
767 ( $c=10^7$  cells/mL) with occasional agitation at 37°C. THP-1 cells were activated for 24 h  
768 with 50 ng/mL PMA (Sigma-Aldrich) prior the infection. THP-1 cells and MDM were

769 infected in the presence of PMA or GM-CSF, respectively, for 16 hours, and also  
770 included a step of centrifugal enhancement of infectivity. UV-inactivation of virus was  
771 performed using a UV crosslinker (HL 2000 hybrilinker) for 3 min at 360 mJ/cm<sup>2</sup>.

772

### 773 **Antibodies**

774 For flow cytometry analysis we used the following anti-mouse antibodies: ICOSL-  
775 biotin or ICOSL-PE (clone HK5.3), MHCI-PE (clone M1/42), B7.1-APC (clone 16-  
776 10A1), CD84-PE (clone mCD84.7), CD11c-A647 or -APC (clone N418), F4/80-PE  
777 (clone BM8), B220-PB (clone RAE-6B2), CD5-PE (clone 53-7.3), CD138-PECy7  
778 (clone 281-2), CD3-A488 (clone 17A2), CD4-PB (clone GK1.5), CXCR5-APC (clone  
779 L138D7), and CD19-A647 (clone 6D5), purchased from Biolegend; CD23-PE (clone  
780 B3B4), CD95-A647 (clone Jo2), CD44-FITC (clone IM7), and CD8-PE (clone 53-6.7),  
781 obtained from BD Biosciences; CD62L-APC (clone MEL-14), CD44-APC or -  
782 AlexaFluor700 (clone IM7), CD21-PECy7 (clone 8D9), GL7-A488 (clone GL7), CD3-  
783 PerCP-Cy5.5 or -PE-eFluor610 (clone 145-2C11), ICOSL-PE (clone HK5.3), B7.1-  
784 APC (clone 16-10A1), CD3-PE-eFluor610 (clone 17A2), CD8-APC, -SuperBright780  
785 or -FITC (clone 53-6.7), CD4-FITC (clone GK1.5), CD45.1-SuperBright600 (clone  
786 A20), CD45.2-eFluor506 (clone 104), CD19-PE-eFluor610 (clone eBio1D3), NKp46-  
787 PE-eFluor610 (clone 29A1.4), CD11b-PE-Cy7 (clone M1/70), CD11c-PerCP-Cy5.5  
788 (clone N418), MHC II-eFluor450 or -APC-eFluor780 (clone M5/114.15.2), TCR V  
789 alpha 11-APC (clone RR8-1 and IFN- $\gamma$  (clone XMG1.2), from eBioscience, Thermo  
790 Fisher Scientific; PD-1-PE (clone J43.1) and CD3-PECy7 (clone 145-2C11), from  
791 Tonbo; and IgM-FITC (polyclonal), from Southern Biotech. Armenian hamster IgG  
792 (clone eBio299 Arm) and rat IgG2a kappa (clone eBR2a) isotype controls were  
793 purchased from Thermo Fisher Scientific. The rat anti-mouse ICOSL (clone HK5.3),

794 anti-mouse NK1.1 (clone PK136), anti-mouse CD8 (clone YTS 169.4), and anti-mouse  
795 CD4 (clone GK1.5) used for the *in vivo* assays were obtained from Bioxcell. The anti-  
796 mouse ICOSL (clone 599841) used for immunochemistry was purchased from  
797 Novusbio Biologicals. Biotin anti-human ICOSL (clone MIH12), CD4-APC (clone  
798 RPA-T4), and CD70 (clone 2F2) were purchased from ThermoFisher, BD Biosciences,  
799 and Immunotools, respectively. Anti-human ICOSL (polyclonal), anti-actin (clone C4),  
800 anti-HA (clone C2974), anti-GFP (polyclonal), and anti-human IE1 (clone 8B1.2), used  
801 for Western blots, were from Elabscience, MP Biomedicals, Cell Signaling MP, Abcam,  
802 and Merck Millipore, respectively. The anti-mouse IE1 (named Croma101) and the anti-  
803 human Fc IgG (clone 29.5; Fc specific) were previously described (Trgovcich et al.,  
804 2000; Pérez-Carmona N et al., 2015). Anti-mouse m04 (clones m04.17 or m04.16)  
805 antibody used as a marker of MCMV infection was produced in the Center for  
806 Proteomics (Faculty of Medicine, University of Rijeka, Croatia), and was described  
807 previously (Železnjak et al., 2019). The anti-mouse IgG-A555 was purchased from Life  
808 Technologies, the anti-rat IgG-A488 and anti-mouse IgG-PE or -A647 from Jackson  
809 ImmunoResearch, the anti-mouse IgG1-PerCP-eFluor710 and anti-mouse IgG2b-FITC  
810 from eBioscience, Thermo Fisher Scientific, the anti-rabbit IgG-HRP from Promega  
811 and the anti-mouse IgG-HRP from Sigma-Aldrich. The streptavidin-PE, -A555, or -  
812 HRP conjugates were purchased from BD Biosciences, ThermoFisher, and Roche,  
813 respectively. The anti-m138 mAb (clone m138.1.120) was generated by fusing an NS1  
814 myeloma cell line with spleen cells from a BALB/c mouse immunized three times with  
815 300.19 cells expressing at the cell surface HA-m138. The m138.1.120 mAb was  
816 subcloned and purified using an Affi-Gel protein A MAPS II kit (Bio-Rad) as indicated  
817 before (Engel et al., 2011). Fixable viability dye eFluor780 and eFluor506 (1000x,  
818 eBioscience, Thermo Fisher Scientific) were used to stain dead cells.



819

## 820 **Plasmid constructions**

821 HA-m138, containing the N-terminal HA-tagged m138 molecule without its signal  
822 peptide, was constructed by PCR using as a template DNA extracted from MCMV  
823 virions and primers m138PstIFor and m138PstIRev. The resulting PCR product was  
824 inserted into the pGEM-T vector, and subsequently, the *m138* fragment was excised  
825 with *Bgl*III and inserted in frame with the HA tag at the N-terminal end into the  
826 mammalian expression vector pDisplay (Invitrogen) opened with *Pst*I. The m138-GFP  
827 plasmid was obtained by PCR employing primers m138BamFor and m138BamRev,  
828 containing a *Bam*HI restriction site, and DNA from MCMV virions as a template. The  
829 PCR product was inserted into the pGEM-T vector, and then the m138 fragment  
830 without its terminal codon was excised with *Bam*HI and inserted in frame with the GFP  
831 at the C-terminal end into the pEGFP-N3 plasmid (clontech) opened with *Bam*HI.  
832 m138ΔIg1-GFP, without the first Ig domain of m138 (322nt-681nt), m138ΔIg2-GFP,  
833 without the second Ig domain of m138 (697nt-1029nt), and m138ΔIg2/3-GFP, without  
834 the second and third Ig domains of m138 (697nt-1416nt), were constructed as follows:  
835 first, independent PCR products were generated using as a template the pEGFP-N3  
836 m138-GFP vector, two common external primers (m138BamFor and m138BamRev),  
837 and for each construct, two internal complementary primers bearing the corresponding  
838 deletions: SOEm138ΔIg1Rev and SOEm138ΔIg1For for m138ΔIg1;  
839 SOEm138ΔIg2Rev and SOEm138ΔIg2For for m138ΔIg2; and SOEm138ΔIg2/3Rev and  
840 SOEm138ΔIg2/3For for m138ΔIg2/3. Splicing by overhang extension (SOE)-PCR was  
841 then performed to join the two PCR fragments obtained for each m138 mutant using the  
842 external primers. These new PCR products were inserted into the pGEM-T vector, and  
843 then fragments of the m138 mutants without their terminal codon stop were excised and

844 cloned in frame with the GFP at the C-terminal end into the pEGFP-N3 plasmid opened  
845 with *Bam*HI. Mouse ICOSL, without its signal peptide, fused to the HA epitope at the  
846 N-terminus (HA-ICOSL) was obtained by PCR employing as a template pCMV6-  
847 mouse ICOSL vector (Origene) and primers ICOSLmurineSalIFor and  
848 ICOSLmurineNotIRev. The resulting PCR product was inserted into the pGEM-T  
849 vector and a *Sal*I-*Not*I fragment corresponding to the murine ICOSL was then excised  
850 and inserted into the mammalian expression vector pDisplay opened with the same  
851 restriction sites. In all cases, the PCR products inserted in the pGEM-T vector were  
852 sequenced to validate the nucleotide sequences, and when required, the correct  
853 orientations of the cloned inserts were assessed employing different restriction sites.

854

#### 855 **Flow cytometry analysis**

856 Flow cytometry was performed according to the Guidelines for the use of flow  
857 cytometry and cell sorting in immunological studies (Cossarizza et al., 2017). To  
858 minimize non specific staining, all incubations were carried out in the presence of 20%  
859 rabbit serum (Linus) and 1% of fetal bovine serum in PBS. Adherent cells were  
860 harvested by incubation with 2 mM EDTA or when indicated by treatment with trypsin  
861 at 37°C. For intracellular staining, cells were fixed and permeabilized with either the  
862 Intracellular fixation & permeabilization buffer set or Foxp3 staining buffer set  
863 (eBioscience) following manufacturer's instructions, before antibody incubations. Prior  
864 to cytometry analysis cell suspensions from spleens, lungs, salivary glands and salivary  
865 gland draining lymph nodes were washed and filtered through a 70 µm cell strainer  
866 (Biologix). All samples were acquired with LSRII Fortessa, FACSAria III or  
867 FACSCanto II flow cytometers (BD Biosciences) and analyzed with FlowJo Xv10.0.7

868 (Tree Star, Inc) software. At least two independent experiments were carried out for  
869 each subject of analysis.

870

#### 871 **Transient and stable transfections**

872 NIH3T3 cells were transiently transfected with 2 µg of the corresponding plasmid using  
873 the Amaxa Cell Line Nucleofactor Kit R according to the manufacturer's protocol.  
874 Likewise, 300.19 and IC-21 cells were transfected employing the Amaxa Cell Line  
875 Nucleofactor Kit V. To generate stable 300.19 cell lines expressing HA-m138 or  
876 NIH3T3 expressing HA-ICOSL, transfections were followed by G418 (Invitrogen)  
877 selection.

878

#### 879 **Western blot analysis**

880 NIH3T3 and THP-1 cells were harvested by scrapping and extracts prepared in lysis  
881 buffer (20 mM Tris-HCl pH 7.5, 1 mM EDTA, 150 mM NaCl and 1% Triton X-100)  
882 supplemented with protease inhibitors (1 mM Na<sub>3</sub>VO<sub>4</sub>, 1 mM PMSF, 0.6 µg/mL  
883 Aprotinin, 2 µg/mL Leupeptin and 312 µg/mL Benzamidin). When specified, cells  
884 were previously incubated with 250 µM leupeptin and 20 nM bafilomycin A1 (Sigma).  
885 Lysates were quantified by a bicinchoninic acid (BCA) protein assay kit  
886 (ThermoScientific), and 15 µg of proteins were subjected to SDS-PAGE in 10%  
887 acrylamide gels and subsequently transferred to nitrocellulose membranes (Protran).  
888 The membranes were incubated with the indicated antibodies and blots were developed  
889 using the SuperSignal West Pico chemiluminescent substrate (Pierce) according to the  
890 manufacturer's protocol. Anti-actin mAb was used as a loading control, and anti-IE1  
891 mAbs were used as infection controls. At least two independent experiments were  
892 carried out for each subject of analysis.

893

#### 894 **Immunoprecipitation**

895 NIH3T3 cells non-transfected or transfected with HA-ICOSL were surface labeled with  
896 biotin (Sigma-Aldrich) and lysed. Cell lysates were precleared 3 times for 30 min  
897 employing protein G-Sepharose (GE Healthcare) and immunoprecipitated by incubation  
898 with an anti-HA agarose conjugate (Sigma-Aldrich). Samples from  
899 immunoprecipitates were subjected to SDS-PAGE and Western blot analysis.  
900 Membranes were incubated with streptavidin-HRP or with anti-HA followed by anti-  
901 rabbit IgG-HRP. At least two independent experiments were carried out for each subject  
902 of analysis.

903

#### 904 **Co-Immunoprecipitation**

905 NIH3T3 cells co-transfected with m138-GFP and HA-ICOSL were lysed with a soft  
906 lysis buffer (20 mM Tris HCl pH 8, 100mM NaCl, 2mM EDTA and 0.5% Triton-X-  
907 100) supplemented with Halt protease inhibitor cocktail, during 30 minutes at 4°C. The  
908 lysates were incubated with G-Sepharose beads in three rounds for 30 minutes each,  
909 followed by an overnight incubation with an anti-HA agarose conjugate. The  
910 immunoprecipitates were washed four times with Co-IP lysis buffer before the samples  
911 were subjected to Western blot analysis. Membranes were incubated with anti-GFP or  
912 with anti-HA, followed by an anti-rabbit IgG-HRP. At least two independent  
913 experiments were carried out for each subject of analysis.

914

#### 915 **Immunofluorescence microscopy**

916 NIH3T3 cells and 300.19 cells, either untransfected or stably transfected with HA-  
917 ICOSL or HA-m138, respectively, were cultured on glass coverslips in 24-well tissue

918 culture plates. When specified, NIH3T3 cells were MCMV infected and exposed to  
919 lysosomal inhibitors as indicated for the Western blot analysis. At 24 hpi, cells were  
920 washed in PBS and fixed and permeabilized using 4% paraformaldehyde and 0.05%  
921 Triton X-100 (for intracellular staining), or just fixed in paraformaldehyde (for cell  
922 surface detection), and subsequently blocked with PBS 6% FBS. Cells were stained  
923 with anti-m138 mAb or anti-ICOSL, using as secondary antibodies an anti-mouse IgG-  
924 A555 or an anti-rat IgG-A488. Nuclei were counterstained with DAPI reagent  
925 (Invitrogen). In assays where the LysoTracker Red DND-99 (Molecular Probes) was  
926 used, cells were incubated at 37°C for 2 hours with 100 nM of the fluorescence dye,  
927 fixed with 4% paraformaldehyde, gently permeabilized with 0.02% saponin, and  
928 immediately processed as indicated above. In this case, the anti-m138 mAb and an anti-  
929 mouse IgG-A488 were used. The samples were mounted in ProLong Gold antifade  
930 reagent (Invitrogen). Cells were examined under a fluorescence microscope at 405 nm  
931 (DAPI), at 555-565 nm (A555), and at 495-518 (A488). GFP was observed at 450-490.  
932 Fluorescence images were obtained using a Nikon Eclipse E600 microscope (Nikon) or  
933 an inverted Leica DMI6000B microscope and the LAS AF software from Leica  
934 Microsystems (Leica, Wetzlar). A Zeiss LSM880 laser scanning spectral confocal  
935 microscope (Zeiss, Jena) equipped with an Axio Observer 7 inverted microscope, blue  
936 diode (405nm), Argon (488nm), diode pumped solid state (561nm) and HeNe (633nm)  
937 lasers and a Plan Apochromat 63x oil (NA 1.4) immersion objective lenses was also  
938 used. DAPI, A-488 and A-555 images were acquired sequentially using 405, 488 and  
939 561 laser lines, AOBS (Acoustic Optical Beam Splitter) as beam splitter and emission  
940 detection ranges 415- 480, 500-550 nm, and 571-625nm, respectively, and the confocal  
941 pinhole set at 1 Airy units. Spectral detection was performed using 2 photomultipliers  
942 and one central GaAsP detector. Analysis of the co-localization of m138 and the

943 LysoTracker red fluorescence was determined using the ImageJ software analyzing 20  
944 cells from each sample. Colocalization was assessed using Coloc2 plugin from  
945 FIJI/ImageJ program (Schindelin et al., 2019). A macro of instructions was created to  
946 process and automate colocalization quantification. Briefly, red and green channel  
947 images were background subtracted with Rolling Ball Radius of 50 and colocalization  
948 was quantified from a region of interest delimiting the cell contour. Manders  
949 coefficients were analyzed from each image. M2 Manders colocalization coefficient  
950 indicates the percentage of m138 colocalizing with lysosomes, and M1 Manders  
951 cocoefficient the percentage of lysosomes colocalizing with m138. At least two  
952 independent experiments were carried out for each subject of analysis.

953

#### 954 **Immunohistochemistry**

955 Mice were euthanized at the indicated time points and spleens immediately collected  
956 within O.C.T. (Sakura) cryo-embedding media at -80°C. Consecutive tissue sections of  
957 2.5 µm were obtained in the cryostat and fixed/permeabilized in acetone. Unspecific  
958 binding was prevented with PBS 6% FBS blocking solution. Antigens were detected  
959 with a rat anti-mouse CD45R/B220 and PNA (peanut lectin) biotin (Sigma-Aldrich).  
960 After 1 hour of incubation at room temperature, B220 antigen was revealed with anti-rat  
961 IgG- A488 and PNA with streptavidin-A555. Labeled tissue sections were visualized  
962 with a fluorescence microscope. Four consecutive tissue sections were evaluated from  
963 three representative mice of each experimental group. Follicle and germinal center areas  
964 were calculated from the total spleen sections of one representative mice of each group  
965 using ImageJ software. At least two independent experiments were carried out for each  
966 subject of analysis.

967

968 **Mouse infections, antibody treatment and determination of viral titers**

969 Four-week-old BALB/c mice (females and males) were obtained from Harlan  
970 (Netherlands) and housed in the vivarium of the Medical School of the University of  
971 Barcelona under specific-pathogen-free (SPF) conditions. Eight-to-twelve-week-old  
972 C57BL/6, TCR transgenic mice specific for M38 (Maxi mice; Torti et al., 2011), TCR  
973 transgenic mice specific for M25-II (Mandaric et al., 2012), C57BL/6 SCID and  
974 BALB/c mice were housed and bred under SPF conditions at the Central Animal  
975 Facility of the Medical Faculty of the University of Rijeka. When specified, ICOSL was  
976 blocked by i.p. injection of a rat anti-mouse ICOSL monoclonal antibody (clone HK5.3)  
977 at a concentration of 100 µg per mouse. The monoclonal antibody was administrated  
978 one day before infection and on days 2, 5, 8 and 11 after infection. The efficacy of the  
979 *in vivo* ICOSL blockade was assessed by cytofluorometric analyses of spleen cells from  
980 treated mice using an anti-ICOSL recognizing the same epitope than the antibody used  
981 in the *in vivo* assay. For these assays, mice were i.p. inoculated with  $2.5 \times 10^6$   
982 PFU/mouse of tissue culture-propagated MCMV $\Delta$ m138. Mice were observed and  
983 weighed during all the experiment and at 14 days post infection, animals were  
984 sacrificed, and specific organs were removed, and their sera collected. Salivary gland  
985 and lungs were harvested as a 10% (weight/volume) tissue homogenate. Tissue  
986 homogenates were sonicated and centrifuged, and viral titers from the supernatants of  
987 individual mice were determined by standard plaque assays in MEFs, including a  
988 centrifugal enhancement of infectivity step. In experiments evaluating the *in vivo* effect  
989 of MCMV infection on ICOSL surface levels, mice were i.p. inoculated with  $2 \times 10^6$   
990 PFU/mouse of MCMV-GFP, and 2 days after infection, cells present in the peritoneal  
991 cavity were harvested with 5 mL of PBS and analyzed by flow cytometry. In depleting  
992 assays, eight-to-twelve-week-old C57BL/6 mice were infected i.v. with  $2 \times 10^5$

993 PFU/mouse of MCMVwt, MCMV $\Delta$ m138, or MCMVm138 $\Delta$ Ig2. On the day of  
994 infection and on days 5<sup>th</sup> and 10<sup>th</sup> after infection, indicated groups of mice were injected  
995 i.p. with 250  $\mu$ g of anti-mouse NK1.1, 150  $\mu$ g of anti-CD8, or 150  $\mu$ g anti-mouse CD4  
996 depleting antibodies. At day 14 post infection, mice were sacrificed and viral titers in  
997 salivary glands and lungs of individual mice were determined by standard plaque  
998 assays. To obtain high-dose systemic infection, BALB/c mice were inoculated i.p. with  
999 10<sup>6</sup> PFU/mouse of MCMVwt or MCMV $\Delta$ m138 for 6 hours after which peritoneal  
1000 exudate cells were isolated according to Ray and Dittel (2010). At least two independent  
1001 experiments were carried out for each subject of analysis.

1002

### 1003 **Adoptive transfer assay**

1004 C57BL/6 SCID mice were i.p. infected with 2x10<sup>5</sup> PFU/mouse of MCMVwt or  
1005 MCMV $\Delta$ m138. One day prior to infection, mice were first injected i.p. with 250  $\mu$ g of  
1006 anti-mouse NK1.1 and a few hours later were given 10<sup>5</sup> M25-II CD4<sup>+</sup> T cells. Another  
1007 NK cell depletion followed on day 3 post infection. Spleen, lungs and salivary glands  
1008 were isolated 7 days after infection and the expansion of CD4<sup>+</sup> T cell (CD45.1<sup>+</sup> CD4<sup>+</sup>)  
1009 was analyzed. M25-II CD4<sup>+</sup> T cells were obtained from naive C57BL/6 transgenic  
1010 M25-II mice. Briefly, splenocytes from C57BL/6 M25-II mice were isolated and  
1011 enriched using CD4<sup>+</sup> T Cell Isolation Kit (Miltenyi). Percentage of M25-II CD4<sup>+</sup> T cells  
1012 was obtained by staining with TCR V alpha 11 (clone RR8-1, eBioscience  
1013 ThermoFisher) antibody.

1014

### 1015 ***In vitro* stimulation of CD8<sup>+</sup> T cells**

1016 C57BL/6 BMDCs were infected with 3 PFU/cell of indicated viruses. After 24 hours of  
1017 infection, splenocytes from naive Maxi mice were added at the different T:E



1018 (BMDCs:CD8<sup>+</sup>) ratios to infected BMDCs together with Brefeldin A (eBioscience,  
1019 Thermo Fisher Scientific). After 6 hours of co-cultivation, IFN- $\gamma$  production by CD8<sup>+</sup> T  
1020 cells was measured. At least three independent experiments were carried out for each  
1021 subject of analysis with two technical replicates/experiment.

1022

### 1023 **Quantification of serum anti-MCMV antibody levels**

1024 Detection of antibodies against MCMV on sera of MCMV-infected mice was performed  
1025 by sandwich ELISA using 1.5  $\mu$ g/well of MCMV $\Delta$ m138-infected MEF lysate to coat  
1026 the ELISA plates as described in Miletic et al., 2017. Briefly, 5x10<sup>6</sup> MEFs were  
1027 infected with 0.01 PFU/cell with MCMV $\Delta$ m138 until a high infection was reached after  
1028 5 days. Cells were then harvested by incubation with 2 mM EDTA and washed twice  
1029 with cold PBS. Cells were sonicated in bicarbonate buffer, quantified by BCA and  
1030 stored at -20°C. Diluted sera were incubated for 2 hours on the coated plates, followed  
1031 by incubation with anti-mouse IgG-HRP to measure total IgGs, or with anti-mouse  
1032 IgG1, IgG2a, IgG2b, IgG3 or IgM biotin conjugated (Jackson ImmunoResearch),  
1033 followed by streptavidin-HRP. After washing, freshly prepared TMB substrate solution  
1034 was added and the absorbance was measured at 450 and 570 nm wavelength (Thermo  
1035 Scientific Multiskan FC). At least two independent experiments were carried out for  
1036 each subject of analysis with at least two technical replicates/experiment.

1037

### 1038 ***In vitro* neutralization**

1039 Collected sera from MCMV infected mice were decomplexed at 56°C for 30  
1040 minutes, and then incubated, at the indicated dilution, with 100 PFU of the MCMV-  
1041 GFP in DMEM containing or not 25% of rabbit serum for 1 hour at 37°C. The mixtures  
1042 were then transferred to monolayers of MEFs p53 grown in wells of 24-well plates, and

1043 further incubated 1 hour at 37°C. Next, cells were covered with medium containing  
1044 0.25% agarose and lysis plaques produced after 5-7 days in each condition counted.  
1045 Results were represented as the percentage of plaque reduction, determined by the ratio  
1046 of the amount of the plaques counted in the sample wells relative to the amount of  
1047 plaques visualized in wells containing the serum of an uninfected mouse. At least two  
1048 independent experiments were carried out for each subject of analysis with at least three  
1049 technical replicates/experiment.

1050

### 1051 **Statistical analyses**

1052 Results are expressed as mean +/- standard deviation (SD) or standard error of the mean  
1053 (SEM) of at least three independent experiments. For *in vivo* experiments, mice were  
1054 pooled and randomized in experimental groups from 4 to 6 animals. The sample size  
1055 was determined by pilot studies and according to the accepted practices in previous  
1056 literature using the MCMV model. The selection of the appropriate statistical test was  
1057 based on the number and distribution of data points per set. Differences between group  
1058 means or individual values were assessed using the unpaired two-tailed *t*-test. Statistical  
1059 differences between more than two study groups were evaluated using either the one-  
1060 way ANOVA test or the Kruskal-Wallis bidirectional test. Exact *p*-values considered  
1061 statistically significant and statistical details of experiments are indicated in the figure  
1062 legends. All statistical analyses were performed using GraphPad Prism software version  
1063 7.03 and 8.1.1.

1064

1065 The key Resources Table (Supplementary File 1) lists the key reagents used in this  
1066 study.

## 1067 **Acknowledgements**

1068 We thank Adriana Lázaro for technical assistance with the production of the  
1069 monoclonal antibody against m138, Manuel Eduardo Sáez Moya for help in the  
1070 preparation of histological tissue sections, and Francesc Poblador and Pablo Hernández-  
1071 Luis for technical assistance in the immunohistochemistry assays. We acknowledge the  
1072 use of the Advanced Optical Microscopy Facility at the University of Barcelona, and  
1073 María Calvo for the analysis of confocal fluorescence microscopy images. We also  
1074 thank Antonio Alcamí (Autonomous University of Madrid, Spain) for providing HSV-1  
1075 and HSV-2 expressing GFP. In addition, we would like to thank Lea Hiršl, Tina Jenuš  
1076 and Maja Cokarić Brdovčak for the help involving adoptive transfer assay and  
1077 genotyping of C57BL/6 M25-II mice.

1078

## 1079 **Competing interests**

1080 No competing interests declared.

1081

## 1082 **Funding**

1083 The study was supported by the Ministerio de Economía y Competitividad (MINECO,  
1084 Spain) through grants SAF 2017-87688 (to Angulo A.), and RTI2018-094440-B-I00 (to  
1085 Engel P.), by the grant “Strengthening the capacity of CerVirVac for research in virus  
1086 immunology and vaccinology“, KK.01.1.1.01.0006, awarded to the Scientific Centre of  
1087 Excellence for Virus Immunology and Vaccines and co-financed by the European  
1088 Regional Development Fund (to Jonjic S.), by the University of Rijeka under the project  
1089 number uniri-biomed-18-170 (to Krmpotić A.), by the Croatian-Swiss Research  
1090 Program of the Croatian Science Foundation and the Swiss National Science  
1091 Foundation with funds obtained from the Swiss-Croatian Cooperation Programme (to

1092 Oxenius A. and Krmpotić A.), and by the Deutsche Forschungsgemeinschaft (DFG,  
1093 German Research Foundation) – Projektnummer 421451057 – FOR2830 (to Messerle  
1094 M. and Jonjic S.) and HE2526/9-1 (to Hengel H.). Angulo G., and Puñet-Ortiz J. were  
1095 supported by a Formación de Personal Investigador fellowship (MINECO).

1096 **References**

1097

1098 Aicher A, Hayden-Ledbetter M, Brady WA, Pezzutto A, Richter G, Magaletti D,  
1099 Buckwalter S, Ledbetter JA, Clark EA. Characterization of human inducible  
1100 costimulator ligand expression and function. *J Immunol.* 2000;164(9):4689-96. DOI:  
1101 [10.4049/jimmunol.164.9.4689](https://doi.org/10.4049/jimmunol.164.9.4689)

1102

1103 Arapović J, Lenac Rovis T, Reddy AB, Krmpotić A, Jonjić S. Promiscuity of MCMV  
1104 immunoevasin of NKG2D: m138/fcr-1 down-modulates RAE-1epsilon in addition to  
1105 MULT-1 and H60. *Mol Immunol.* 2009;47(1):114-22. DOI:  
1106 [10.1016/j.molimm.2009.02.010](https://doi.org/10.1016/j.molimm.2009.02.010)

1107

1108 Arens R, Loewendorf A, Her MJ, Schneider-Ohrum K, Shellam GR, Janssen E, Ware  
1109 CF, Schoenberger SP, Benedict CA. B7-mediated costimulation of CD4 T cells  
1110 constrains cytomegalovirus persistence. *J Virol.* 2011;85(1):390-6.  
1111 DOI:[10.1128/JVI.01839-10](https://doi.org/10.1128/JVI.01839-10)

1112

1113 Bertram EM, Tafuri A, Shahinian A, Chan VS, Hunziker L, Recher M, Ohashi PS, Mak  
1114 TW, Watts TH. Role of ICOS versus CD28 in antiviral immunity. *Eur J Immunol.*  
1115 2002;32(12):3376-85. DOI:[10.1002/1521-4141\(200212\)32:12<3376::AID-  
1116 IMMU3376>3.0.CO;2-Y](https://doi.org/10.1002/1521-4141(200212)32:12<3376::AID-IMMU3376>3.0.CO;2-Y)

1117

1118 Brinkmann MM, Dağ F, Hengel H, Messerle M, Kalinke U, Čičin-Šain L.  
1119 Cytomegalovirus immune evasion of myeloid lineage cells. *Med Microbiol Immunol.*  
1120 2015;204(3):367-82. DOI:[10.1007/s00430-015-0403-4](https://doi.org/10.1007/s00430-015-0403-4)

1121

1122 Brune W, Wagner M, Messerle M. Manipulating cytomegalovirus genomes by BAC  
1123 mutagenesis: Strategies and applications, *in* Reddehase, M.J. (*ed.*) Cytomegaloviruses,  
1124 Molecular Biology and Immunology. (Vol. 1). Caister Academic Press. Norfolk, UK.  
1125 2006;63-89.

1126

1127 Budt M, Reinhard H, Bigl A, Hengel H. Herpesviral Fcγ receptors: culprits  
1128 attenuating antiviral IgG? *Int Immunopharmacol.* 2004;4(9):1135-48.  
1129 DOI:[10.1016/j.intimp.2004.05.020](https://doi.org/10.1016/j.intimp.2004.05.020)

1130

1131 Cavanaugh VJ, Stenberg RM, Staley TL, Virgin HW 4th, MacDonald MR, Paetzold S,  
1132 Farrell HE, Rawlinson WD, Campbell AE. Murine cytomegalovirus with a deletion of  
1133 genes spanning HindIII-J and -I displays altered cell and tissue tropism. *J Virol.*  
1134 1996;70(3):1365-74.

1135

1136 Chen L, Flies DB. Molecular mechanisms of T cell co-stimulation and co-inhibition.  
1137 *Nat Rev Immunol.* 2013;13(4):227-42. DOI:[10.1038/nri3405](https://doi.org/10.1038/nri3405)

1138

1139 Choi YS, Kageyama R, Eto D, Escobar TC, Johnston RJ, Monticelli L, Lao C, Crotty S.  
1140 ICOS receptor instructs T follicular helper cell versus effector cell differentiation via  
1141 induction of the transcriptional repressor Bcl6. *Immunity.* 2011;34(6):932-46.  
1142 DOI:[10.1016/j.immuni.2011.03.023](https://doi.org/10.1016/j.immuni.2011.03.023)

1143

1144 Clement M, Marsden M, Stacey MA, Abdul-Karim J, Gimeno Brias S, Costa Bento D,  
1145 Scurr MJ, Ghazal P, Weaver CT, Carlesso G, Clare S, Jones SA, Godkin A, Jones GW,

1146 Humphreys IR. Cytomegalovirus-specific IL-10-Producing CD4+ T Cells are governed  
1147 by type-I IFN-induced IL-27 and promote virus persistence. PLoS Pathog.  
1148 2016;12(12):e1006050. DOI: [10.1371/journal.ppat.1006050](https://doi.org/10.1371/journal.ppat.1006050)  
1149

1150 Corrales-Aguilar E, Hoffmann K, Hengel H. CMV-encoded Fcγ receptors: modulators  
1151 at the interface of innate and adaptive immunity. Semin Immunopathol.  
1152 2014;36(6):627-40.  
1153 DOI: [10.1007/s00281-014-0448-2](https://doi.org/10.1007/s00281-014-0448-2)  
1154

1155 Cossarizza A, Chang HD, Radbruch A, Acs A, Adam D, Adam-Klages S, et al.  
1156 Guidelines for the use of flow cytometry and cell sorting in immunological studies  
1157 (second edition). Eur J Immunol. 2019;49(10):1457-973. DOI: [10.1002/eji.201970107](https://doi.org/10.1002/eji.201970107)  
1158

1159 Coyle AJ, Lehar S, Lloyd C, Tian J, Delaney T, Manning S, Nguyen T, Burwell T,  
1160 Schneider H, Gonzalo JA, Gosselin M, Owen LR, Rudd CE, Gutierrez-Ramos JC. The  
1161 CD28-related molecule ICOS is required for effective T cell-dependent immune  
1162 responses. Immunity. 2000;13(1):95-105. DOI: [10.1016/s1074-7613\(00\)00011-x](https://doi.org/10.1016/s1074-7613(00)00011-x)  
1163

1164 Crnković-Mertens I, Messerle M, Milotić I, Szepan U, Kucić N, Krmpotić A, Jonjić S,  
1165 Koszinowski UH. Virus attenuation after deletion of the cytomegalovirus Fc receptor  
1166 gene is not due to antibody control. J Virol. 1998;72(2):1377-82.  
1167

1168 Engel P, Pérez-Carmona N, Albà MM, Robertson K, Ghazal P, Angulo A. Human  
1169 cytomegalovirus UL7, a homologue of the SLAM-family receptor CD229, impairs  
1170 cytokine production. Immunol Cell Biol. 2011;89(7):753-66. DOI: [10.1038/icb.2011.55](https://doi.org/10.1038/icb.2011.55)

1171

1172 Fielding CA, Weekes MP, Nobre LV, Ruckova E, Wilkie GS, Paulo JA, Chang C,  
1173 Suárez NM, Davies JA, Antrobus R, Stanton RJ, Aicheler RJ, Nichols H, Vojtesek B,  
1174 Trowsdale J, Davison AJ, Gygi SP, Tomasec P, Lehner PJ, Wilkinson GW. Control of  
1175 immune ligands by members of a cytomegalovirus gene expansion suppresses natural  
1176 killer cell activation. *Elife*. 2017;6. pii: e22206. DOI:[10.7554/eLife.22206](https://doi.org/10.7554/eLife.22206)

1177

1178 Fink A, Renzaho A, Reddehase MJ, Lemmermann NA. The p36 isoform of murine  
1179 cytomegalovirus m152 protein suffices for mediating innate and adaptive immune  
1180 evasion. *Viruses*. 2013;5(12):3171-91. DOI: [10.3390/v5123171](https://doi.org/10.3390/v5123171)

1181

1182 Fleming P, Davis-Poynter N, Degli-Esposti M, Densley E, Papadimitriou J, Shellam G,  
1183 Farrell H. The murine cytomegalovirus chemokine homolog, m131/129, is a  
1184 determinant of viral pathogenicity. *J Virol*. 1999;73(8):6800-9. DOI:  
1185 [10.1128/JVI.73.8.6800-6809.1999](https://doi.org/10.1128/JVI.73.8.6800-6809.1999)

1186

1187 Gewurz BE, Vyas JM, Ploegh HL. Herpesvirus evasion of T-cell immunity. In: Arvin  
1188 A, Campadelli-Fiume G, Mocarski E, Moore PS, Roizman B, Whitley R, Yamanishi K,  
1189 editors. *Human Herpesviruses: Biology, Therapy, and Immunoprophylaxis*. Cambridge:  
1190 Cambridge University Press. 2007. Chapter 62. PubMed PMID: 21348103.

1191

1192 Hertel L, Lacaille VG, Strobl H, Mellins ED, Mocarski ES. Susceptibility of immature  
1193 and mature Langerhans cell-type dendritic cells to infection and immunomodulation by  
1194 human cytomegalovirus. *J Virol*. 2003;77(13):7563-74. DOI:[10.1128/jvi.77.13.7563-  
1195 7574.2003](https://doi.org/10.1128/jvi.77.13.7563-7574.2003)



1196

1197 Hudson JB. Further studies on the mechanism of centrifugal enhancement of  
1198 cytomegalovirus infectivity. *J Virol Methods*. 1988;19(2):97-108. DOI:[10.1016/0166-](https://doi.org/10.1016/0166-0934(88)90153-x)  
1199 [0934\(88\)90153-x](https://doi.org/10.1016/0166-0934(88)90153-x)

1200

1201 Hutloff A, Dittrich AM, Beier KC, Eljaschewitsch B, Kraft R, Anagnostopoulos I,  
1202 Kroczek RA. ICOS is an inducible T-cell co-stimulator structurally and functionally  
1203 related to CD28. *Nature*. 1999;397(6716):263-6. DOI:[10.1038/16717](https://doi.org/10.1038/16717)

1204

1205 Hutloff A. Regulation of T follicular helper cells by ICOS. *Oncotarget*.  
1206 2015;6(26):21785-6. DOI: [10.18632/oncotarget.4798](https://doi.org/10.18632/oncotarget.4798)

1207

1208 Khan N, Gowthaman U, Pahari S, Agrewala JN. Manipulation of costimulatory  
1209 molecules by intracellular pathogens: veni, vidi, vici!! *PLoS Pathog*.  
1210 2012;8(6):e1002676. DOI:[10.1371/journal.ppat.1002676](https://doi.org/10.1371/journal.ppat.1002676)

1211

1212 Khayyamian S, Hutloff A, Büchner K, Gräfe M, Henn V, Kroczek RA, Mages HW.  
1213 ICOS-ligand, expressed on human endothelial cells, costimulates Th1 and Th2 cytokine  
1214 secretion by memory CD4+ T cells. *Proc Natl Acad Sci U S A*. 2002;99(9):6198-203.  
1215 DOI:[10.1073/pnas.092576699](https://doi.org/10.1073/pnas.092576699)

1216

1217 Kopf M, Coyle AJ, Schmitz N, Barner M, Oxenius A, Gallimore A, Gutierrez-Ramos  
1218 JC, Bachmann MF. Inducible costimulator protein (ICOS) controls T helper cell subset  
1219 polarization after virus and parasite infection. *J Exp Med*. 2000;192(1):53-61.  
1220 DOI:[10.1084/jem.192.1.53](https://doi.org/10.1084/jem.192.1.53)

1221

1222 Krmpotić A, Messerle M, Crnkovic-Mertens I, Polic B, Jonjic S, Koszinowski UH. The  
1223 immunoevasive function encoded by the mouse cytomegalovirus gene m152 protects  
1224 the virus against T cell control in vivo. *J Exp Med.* 1999;190(9):1285-96.  
1225 DOI: [10.1084/jem.190.9.1285](https://doi.org/10.1084/jem.190.9.1285)

1226

1227 Lenac T, Budt M, Arapović J, Hasan M, Zimmermann A, Simic H, Krmpotic A,  
1228 Messerle M, Ruzsics Z, Koszinowski UH, Hengel H, Jonjic S. The herpesviral Fc  
1229 receptor fcr-1 down-regulates the NKG2D ligands MULT-1 and H60. *J Exp Med.*  
1230 2006;203(8):1843-50. DOI:[10.1084/jem.20060514](https://doi.org/10.1084/jem.20060514)

1231

1232 Liu D, Xu H, Shih C, Wan Z, Ma X, Ma W, Luo D, Qi H. T-B-cell entanglement and  
1233 ICOSL-driven feed-forward regulation of germinal centre reaction. *Nature.*  
1234 2015;517(7533):214-8. DOI:[10.1038/nature13803](https://doi.org/10.1038/nature13803)

1235

1236 Lodoen M, Ogasawara K, Hamerman JA, Arase H, Houchins JP, Mocarski ES, Lanier  
1237 LL. NKG2D-mediated natural killer cell protection against cytomegalovirus is impaired  
1238 by viral gp40 modulation of retinoic acid early inducible 1 gene molecules. *J Exp Med.*  
1239 2003;197(10):1245-53. DOI:[10.1084/jem.20021973](https://doi.org/10.1084/jem.20021973)

1240

1241 Loewendorf A, Krüger C, Borst EM, Wagner M, Just U, Messerle M. Identification of a  
1242 mouse cytomegalovirus gene selectively targeting CD86 expression on antigen-  
1243 presenting cells. *J Virol.* 2004;78(23):13062-71. DOI: [10.1128/JVI.78.23.13062-](https://doi.org/10.1128/JVI.78.23.13062-13071.2004)  
1244 [13071.2004](https://doi.org/10.1128/JVI.78.23.13062-13071.2004)

1245

1246 Mandaric S, Walton SM, Rüllicke T, Richter K, Girard-Madoux MJ, Clausen BE,  
1247 Zurunic A, Kamanaka M, Flavell RA, Jonjic S, Oxenius A. IL-10 suppression of  
1248 NK/DC crosstalk leads to poor priming of MCMV-specific CD4 T cells and prolonged  
1249 MCMV persistence. PLoS Pathog. 2012;8(8):e1002846. DOI:  
1250 [10.1371/journal.ppat.1002846](https://doi.org/10.1371/journal.ppat.1002846)  
1251  
1252 Mathys S, Schroeder T, Ellwart J, Koszinowski UH, Messerle M, Just U. Dendritic cells  
1253 under influence of mouse cytomegalovirus have a physiologic dual role: to initiate and  
1254 to restrict T cell activation. J Infect Dis. 2003;187(6):988-99. DOI:[10.1086/368094](https://doi.org/10.1086/368094)  
1255  
1256 Miletic A, Lenartic M, Popovic B, Brizic I, Trsan T, Miklic K, Mandelboim O,  
1257 Krmpotic A, Jonjic S. NCR1-deficiency diminishes the generation of protective murine  
1258 cytomegalovirus antibodies by limiting follicular helper T-cell maturation. Eur J  
1259 Immunol. 2017;47(9):1443-56. DOI:[10.1002/eji.201646763](https://doi.org/10.1002/eji.201646763)  
1260  
1261 Mintern JD, Klemm EJ, Wagner M, Paquet ME, Napier MD, Kim YM, Koszinowski  
1262 UH, Ploegh HL. Viral interference with B7-1 costimulation: a new role for murine  
1263 cytomegalovirus  $\gamma$ 1 receptor-1. J Immunol. 2006;177(12):8422-31.  
1264 DOI:[10.4049/jimmunol.177.12.8422](https://doi.org/10.4049/jimmunol.177.12.8422)  
1265  
1266 Moutaftsi M, Mehl AM, Borysiewicz LK, Tabi Z. Human cytomegalovirus inhibits  
1267 maturation and impairs function of monocyte-derived dendritic cells. Blood.  
1268 2002;99(8):2913-21. DOI:[10.1182/blood.v99.8.2913](https://doi.org/10.1182/blood.v99.8.2913)  
1269

1270 Ogasawara K, Yoshinaga SK, Lanier LL. Inducible costimulator costimulates cytotoxic  
1271 activity and IFN-gamma production in activated murine NK cells. *J Immunol.*  
1272 2002;169(7):3676-85. DOI:[10.4049/jimmunol.169.7.3676](https://doi.org/10.4049/jimmunol.169.7.3676)  
1273

1274 Pérez-Carmona N, Farré D, Martínez-Vicente P, Terhorst C, Engel P, Angulo A.  
1275 Signaling lymphocytic activation molecule family receptor homologs in new world  
1276 monkey cytomegaloviruses. *J Virol.* 2015;89:11323-36. DOI:[10.1128/JVI.01296-15](https://doi.org/10.1128/JVI.01296-15)  
1277

1278 Qian X, Agematsu K, Freeman GJ, Tagawa Y, Sugane K, Hayashi T. The ICOS-ligand  
1279 B7-H2, expressed on human type II alveolar epithelial cells, plays a role in the  
1280 pulmonary host defense system. *Eur J Immunol.* 2006;36(4):906-18.  
1281 DOI:[10.1002/eji.200535253](https://doi.org/10.1002/eji.200535253)  
1282

1283 Ray A, Dittel BN. Isolation of mouse peritoneal cavity cells. *J Vis Exp.* 2010;(35):1488.  
1284 DOI:[10.3791/1488](https://doi.org/10.3791/1488)  
1285

1286 Riley JL, Mao M, Kobayashi S, Biery M, Burchard J, Cavet G, Gregson BP, June CH,  
1287 Linsley PS. Modulation of TCR-induced transcriptional profiles by ligation of CD28,  
1288 ICOS, and CTLA-4 receptors. *Proc Natl Acad Sci U S A.* 2002;99(18):11790-5.  
1289 DOI:[10.1073/pnas.162359999](https://doi.org/10.1073/pnas.162359999)  
1290

1291 Roussel L, Landekic M, Golizeh M, Gavino C, Zhong MC, Chen J, Faubert D,  
1292 Blanchet-Cohen A, Dansereau L, Parent MA, Marin S, Luo J, Le C, Ford BR, Langelier  
1293 M, King IL, Divangahi M, Foulkes WD, Veillette A, Vinh DC. Loss of human ICOSL  
1294 results in combined immunodeficiency. *J Exp Med.* 2018;215(12):3151-64.

1295 DOI:[10.1084/jem.20180668](https://doi.org/10.1084/jem.20180668)  
1296  
1297 Schepp J, Chou J, Skrabl-Baumgartner A, Arkwright PD, Engelhardt KR, Hambleton S,  
1298 Morio T, Röther E, Warnatz K, Geha R, Grimbacher B. 14 Years after discovery:  
1299 clinical follow-up on 15 patients with inducible co-stimulator deficiency. *Front*  
1300 *Immunol.* 2017;8:964. DOI:[10.3389/fimmu.2017.00964](https://doi.org/10.3389/fimmu.2017.00964)  
1301  
1302 Schindelin J, Arganda-Carreras I, Frise E, Kaynig V, Longair M, Pietzsch T, Preibisch  
1303 S, Rueden C, Saalfeld S, Schmid B, Tinevez JY, White DJ, Hartenstein V, Eliceiri K,  
1304 Tomancak P, Cardona A. Fiji: an open-source platform for biological-image analysis.  
1305 *Nat Methods.* 2012 28;9(7):676-82. DOI: [10.1038/nmeth.2019](https://doi.org/10.1038/nmeth.2019)  
1306  
1307 Schuren AB, Costa AI, Wiertz EJ. Recent advances in viral evasion of the MHC Class I  
1308 processing pathway. *Curr Opin Immunol.* 2016;40:43-50.  
1309 DOI:[10.1016/j.coi.2016.02.007](https://doi.org/10.1016/j.coi.2016.02.007)  
1310  
1311 Sharpe AH, Freeman GJ. The B7-CD28 superfamily. *Nat Rev Immunol.* 2002;2(2):116-  
1312 26. DOI:[10.1038/nri727](https://doi.org/10.1038/nri727)  
1313  
1314 Sharpe AH. Mechanisms of costimulation. *Immunol Rev.* 2009;229(1):5-11.  
1315 DOI: [10.1111/j.1600-065X.2009.00784.x](https://doi.org/10.1111/j.1600-065X.2009.00784.x)  
1316  
1317 Sinzger C, Hahn G, Digel M, Katona R, Sampaio KL, Messerle M, Hengel H,  
1318 Koszinowski U, Brune W, Adler B. Cloning and sequencing of a highly productive,

1319 endotheliotropic virus strain derived from human cytomegalovirus TB40/E. *J Gen*  
1320 *Virol.* 2008;89(Pt 2):359-68. DOI:[10.1099/vir.0.83286-0](https://doi.org/10.1099/vir.0.83286-0)

1321

1322 Stahl FR, Keyser KA, Heller K, Bischoff Y, Halle S, Wagner K, Messerle M, Förster R.  
1323 Mck2-dependent infection of alveolar macrophages promotes replication of MCMV in  
1324 nodular inflammatory foci of the neonatal lung. *Mucosal Immunol.* 2015;8(1):57-  
1325 67. DOI:[10.1038/mi.2014.42](https://doi.org/10.1038/mi.2014.42)

1326

1327 Stempel M, Chan B, Juranić Lisnić V, Krmpotić A, Hartung J, Paludan SR, Füllbrunn  
1328 N, Lemmermann NA, Brinkmann MM. The herpesviral antagonist m152 reveals  
1329 differential activation of STING-dependent IRF and NF- $\kappa$ B signaling and STING's dual  
1330 role during MCMV infection. *EMBO J.* 2019;38(5). pii: e100983.  
1331 DOI:[10.15252/embj.2018100983](https://doi.org/10.15252/embj.2018100983)

1332

1333 Strazić Geljić I, Kucan Brlić P, Angulo G, Brizic I, Lisnić B, Jenus T, Juranić Lisnić V,  
1334 Pietri GP, Engel P, Kaynan N, Zeleznjak J, Schu P, Mandelboim O, Krmpotić A,  
1335 Angulo A, Jonjić S, Lenac Rovis T. Cytomegalovirus protein m154 perturbs the adaptor  
1336 protein-1 compartment mediating broad-spectrum immune evasion. *Elife.* 2020;9. pii:  
1337 e50803. DOI:[10.7554/eLife.50803](https://doi.org/10.7554/eLife.50803)

1338

1339 Swallow MM, Wallin JJ, Sha WC. B7h, a novel costimulatory homolog of B7.1 and  
1340 B7.2, is induced by TNF $\alpha$ . *Immunity.* 1999;11(4):423-32. DOI:[10.1016/s1074-](https://doi.org/10.1016/s1074-7613(00)80117-x)  
1341 [7613\(00\)80117-x](https://doi.org/10.1016/s1074-7613(00)80117-x)

1342

1343 Takahashi N, Matsumoto K, Saito H, Nanki T, Miyasaka N, Kobata T, Azuma M, Lee  
1344 SK, Mizutani S, Morio T. Impaired CD4 and CD8 effector function and decreased  
1345 memory T cell populations in ICOS-deficient patients. *J Immunol.* 2009;182(9):5515-  
1346 27.  
1347 DOI:[10.4049/jimmunol.0803256](https://doi.org/10.4049/jimmunol.0803256)  
1348  
1349 Tesciuba AG, Subudhi S, Rother RP, Faas SJ, Frantz AM, Elliot D, Weinstock J, Matis  
1350 LA, Bluestone JA, Sperling AI. Inducible costimulator regulates Th2-mediated  
1351 inflammation, but not Th2 differentiation, in a model of allergic airway disease. *J*  
1352 *Immunol.* 2001;167(4):1996-2003. DOI:[10.4049/jimmunol.167.4.1996](https://doi.org/10.4049/jimmunol.167.4.1996)  
1353  
1354 Thäle R, Lucin P, Schneider K, Eggers M, Koszinowski UH. Identification and  
1355 expression of a murine cytomegalovirus early gene coding for an Fc receptor. *J Virol.*  
1356 1994;68(12):7757-65.  
1357  
1358 Torti N, Walton SM, Brocker T, Rüllicke T, Oxenius A. 2011. Non-hematopoietic cells  
1359 in lymph nodes drive memory CD8 T cell inflation during murine cytomegalovirus  
1360 infection. *PLoS Pathog.* 2011;7:e1002313. DOI: [10.1371/journal.ppat.1002313](https://doi.org/10.1371/journal.ppat.1002313)  
1361  
1362 Trgovcich J, Stimac D, Polić B, Krmpotić A, Pernjak-Pugel E, Tomac J, Hasan M,  
1363 Wraber B, Jonjić S. Immune responses and cytokine induction in the development of  
1364 severe hepatitis during acute infections with murine cytomegalovirus. *Arch Virol.*  
1365 2000;145(12):2601-18. DOI:[10.1007/s007050070010](https://doi.org/10.1007/s007050070010)  
1366

1367 Wagner M, Jonjic S, Koszinowski UH, Messerle M. Systematic excision of vector  
1368 sequences from the BAC-cloned herpesvirus genome during virus reconstitution. *J*  
1369 *Virool.* 1999;73(8):7056-60.  
1370  
1371 Wallin JJ, Liang L, Bakardjiev A, Sha WC. Enhancement of CD8+ T cell responses by  
1372 ICOS/B7h costimulation. *J Immunol.* 2001;167(1):132-9.  
1373 DOI:[10.4049/jimmunol.167.1.132](https://doi.org/10.4049/jimmunol.167.1.132)  
1374  
1375 Welten SPM, Redeker A, Toes REM, Arens R. Viral persistence induces antibody  
1376 inflation without altering antibody avidity. *J Virool.* 2016;90(9):4402-11.  
1377 DOI:[10.1128/JVI.03177-15](https://doi.org/10.1128/JVI.03177-15)  
1378  
1379 Wikenheiser DJ, Stumhofer JS. ICOS Co-Stimulation: Friend or Foe? *Front Immunol.*  
1380 2016;7:304. DOI:[10.3389/fimmu.2016.00304](https://doi.org/10.3389/fimmu.2016.00304)  
1381  
1382 Yoshinaga SK, Whoriskey JS, Khare SD, Sarmiento U, Guo J, Horan T, Shih G, Zhang  
1383 M, Coccia MA, Kohno T, Tafuri-Bladt A, Brankow D, Campbell P, Chang D, Chiu L,  
1384 Dai T, Duncan G, Elliott GS, Hui A, McCabe SM, Scully S, Shahinian A, Shaklee CL,  
1385 Van G, Mak TW, Senaldi G. T-cell co-stimulation through B7RP-1 and ICOS. *Nature.*  
1386 1999;402(6763):827-32. DOI:[10.1038/45582](https://doi.org/10.1038/45582)  
1387  
1388 Yoshinaga SK, Zhang M, Pistillo J, Horan T, Khare SD, Miner K, Sonnenberg M,  
1389 Boone T, Brankow D, Dai T, Delaney J, Han H, Hui A, Kohno T, Manoukian R,  
1390 Whoriskey JS, Coccia MA. Characterization of a new human B7-related protein: B7RP-



1391 1 is the ligand to the co-stimulatory protein ICOS. *Int Immunol.* 2000;12(10):1439-47.  
1392 DOI:[10.1093/intimm/12.10.1439](https://doi.org/10.1093/intimm/12.10.1439)  
1393  
1394 Zarama A, Pérez-Carmona N, Farré D, Tomic A, Borst EM, Messerle M, Jonjic S,  
1395 Engel P, Angulo A. Cytomegalovirus m154 hinders CD48 cell-surface expression and  
1396 promotes viral escape from host natural killer cell control. *PLoS Pathog.*  
1397 2014;10(3):e1004000. DOI:[10.1371/journal.ppat.1004000](https://doi.org/10.1371/journal.ppat.1004000)  
1398  
1399 Železnjak J, Lisnić VJ, Popović B, Lisnic B, Babic M, Halenius A, L'Hernault A, Lenac  
1400 Rovis A, Hengel H, Erhard F, Redwood AJ, Vidal SM, Dölken L, Krmpotić A, Jonjic  
1401 S. The complex of MCMV proteins and MHC class I evades NK cell control and drives  
1402 the evolution of virus-specific activating Ly49 receptors. *J Exp Med.* 2019;216(8):1809-  
1403 27. DOI: [10.1084/jem.20182213](https://doi.org/10.1084/jem.20182213)  
1404  
1405 Ziegler H, Thale R, Lucin P, Muranyi W, Flohr T, Hengel H, Farrell H, Rawlinson W,  
1406 Koszinowski UH. A mouse cytomegalovirus glycoprotein retains MHC class I  
1407 complexes in the ERGIC/cis-Golgi compartments. *Immunity.* 1997;6(1):57-66. DOI:  
1408 [10.1016/s1074-7613\(00\)80242-3](https://doi.org/10.1016/s1074-7613(00)80242-3)

1409 **Figure legends**

1410

1411 **Figure 1. Downregulation of ICOSL upon MCMV infection of APCs.** (A) Peritoneal  
1412 macrophages (MΦ) were mock-infected or infected for 72 hours with MCMV-GFP at  
1413 an moi of 5 and analyzed by flow cytometry for surface expression of ICOSL, MHC I,  
1414 or CD62L using specific mAbs against each of these molecules. Grey histograms  
1415 represent the expression on mock-infected cells, green histograms represent the  
1416 expression on MCMV-infected (GFP+) cells, and blue histograms represent the  
1417 expression on uninfected (GFP-) cells from the same culture. (B) Bone marrow derived-  
1418 macrophages (BMM), bone marrow derived-dendritic cells (BMDC), IC-21, DC2.4,  
1419 and SVEC4-10 cells were infected with MCMV-GFP at different moi (10, 20, 20, and  
1420 5, respectively) to obtain an infection of around 50% of the cell culture, and analyzed by  
1421 flow cytometry for surface expression of ICOSL. Grey, green, and blue histograms, as  
1422 indicated in A. (C) Same as in A, except that peritoneal macrophages were infected with  
1423 MCMV-GFP at an moi of 10, or treated for 72 h with the same amount of MCMV-GFP  
1424 UV-inactivated. Grey and green as indicated in A, and red histograms represent the  
1425 expression on MCMV-GFP UV-inactivated infected cells. (D) Peritoneal macrophages,  
1426 BMDCs, and IC-21 cells were mock-infected (time 0) or infected with MCMV-GFP at  
1427 an moi of 10, 40 and 20, respectively, and analyzed by flow cytometry for surface  
1428 expression of ICOSL at the different time points after infection indicated. In A, B, C,  
1429 and D, the isotype for each antibody was used as a negative control (dotted lines). Data  
1430 are representative of at least two independent experiments.

1431

1432 **Figure 2. Identification of the MCMV gene involved in the decreased cell surface**  
1433 **expression of ICOSL.** (A) IC-21 cells were mock-infected or infected for 72 h with

1434 MCMV-GFP, MCMV-GFP $\Delta$ m128-m138, or MCMV-GFP $\Delta$ m1-m17 at an moi of 10  
1435 and examined by flow cytometry for surface expression of ICOSL. Grey histograms  
1436 represent the expression of mock-infected cells, green histograms represent the  
1437 expression on MCMV-infected (GFP+) cells, and blue histograms represent the  
1438 expression on uninfected (GFP-) cells from the same culture. (B) IC-21 cells were  
1439 mock-infected or infected with MCMVwt or MCMV $\Delta$ m138 for 72h at an moi of 20 and  
1440 analyzed by flow cytometry for surface expression of ICOSL and CD84. Grey  
1441 histograms as indicated in A, and brown histograms represent the expression on  
1442 MCMVwt and MCMV $\Delta$ m138 IC-21 infected cells. (C) IC-21 cells were mock-  
1443 transfected or transfected with the m138-GFP construct or with the control GFP empty  
1444 vector and stained with the anti-ICOSL mAb or an isotype control (dotted lines). Dark  
1445 green and red histograms represent cells from transfected cultures expressing or not  
1446 expressing GFP, respectively, and grey histograms represent surface expression of  
1447 ICOSL on untransfected cells. In A, B, and C, the isotype for each antibody was used as  
1448 a negative control (dotted lines). Data are representative of at least two independent  
1449 experiments.

1450

1451 **Figure 3. Localization of m138 in MCMV infected cells.** (A) NIH3T3 cells were  
1452 infected with MCMV-GFP at an moi of 5 for 24 h, fixed with 4% formaldehyde (panels  
1453 d-f) or fixed and permeabilized with 0.05% Triton (panels a-c and g), and stained with  
1454 the anti-m138 mAb followed by an anti-mouse IgG-A555. Nuclei were stained with the  
1455 DAPI reagent. The cells were examined under a fluorescence microscope.  
1456 Magnification, x20 (a-f); an enlarged individual cell from panel c is shown in panel g.  
1457 (B) MCMVwt-infected NIH3T3 cells were examined by flow cytometry for surface  
1458 expression of m138 with the anti-m138 mAb (red histogram). Dotted line represents the

1459 isotype control. (C) 300.19 cells untransfected or stably transfected with the HA-m138  
1460 construct were fixed with 4% formaldehyde and stained with the anti-m138 mAb and  
1461 DAPI and examined under a fluorescence microscope as indicated in A. Magnification,  
1462 x20. Overlaid images are shown. Transfected cells from the same cultures were  
1463 analyzed by flow cytometry (right panels) with the anti-m138 mAb (red histogram), an  
1464 anti-HA mAb (grey histogram) or isotype controls (dotted lines). (D) NIH3T3 cells  
1465 were infected with MCMV at an moi of 5 for 24 h, treated with LysoTracker DND99,  
1466 fixed with 4% formaldehyde and permeabilized with 0.02% Saponin, and stained with  
1467 the anti-m138 mAb followed by an anti-mouse IgG-A488. Nuclei were stained with the  
1468 DAPI reagent. The cells were examined under a confocal microscope. Representative  
1469 fields are shown in panels a, b, and c, with an enlargement of an individual and more  
1470 exposed cell from panel c, in panel d. Magnification, x63.

1471 The online version of this article includes the following figure supplements for figure 3:  
1472 Figure supplement 1. **Localization of m138 in MCMV-infected DC2.4 cells.**

1473

1474 **Figure 4. m138 leads to a reduction of the expression of ICOSL on the cell surface**  
1475 **of infected cells but not of its overall intracellular levels.** (A) NIH3T3 cells stably  
1476 transfected with HA-ICOSL were mock-infected (grey histograms) or infected with  
1477 MCMVwt or MCMV $\Delta$ m138 (brown or pink histograms, respectively) and analyzed by  
1478 flow cytometry for surface expression of ICOSL and MHC I. (B) NIH3T3 HA-ICOSL  
1479 cells non-transfected (grey histograms) or transfected with the m138-GFP construct  
1480 (green histograms) were analyzed by flow cytometry for surface expression of ICOSL  
1481 and CD44. In A and B, the isotype for each antibody was used as a negative control  
1482 (dotted lines). (C) NIH3T3 HA-ICOSL cells were mock-infected (lane 2), treated with  
1483 trypsin (lane 3), or infected with MCMVwt (lane 4) or MCMV $\Delta$ m138 (lane 5).

1484 Untransfected NIH3T3 cells were used as a control (lane 1). Samples were analyzed by  
1485 western blot using an anti-HA mAb, followed by anti-rabbit IgG-HRP. An anti-IE1 and  
1486 an anti-actin mAbs followed by anti-mouse IgG-HRP, were used as controls of MCMV  
1487 infection and loading, respectively. (D) Flow cytometry analysis of NIH3T3 HA-  
1488 ICOSL treated with trypsin (open histogram) or mock-treated (grey histogram) and  
1489 stained with an anti-HA mAb or an isotype control (dotted line), followed by anti-  
1490 mouse IgG PE. (E) NIH3T3 cells (lane 1) or NIH3T3 HA-ICOSL (lane 2) were surface  
1491 labeled with biotin, immunoprecipitated with an anti-HA mAb, and analyzed by western  
1492 blot analysis using streptavidin-HRP conjugate. (F) NIH3T3 HA-ICOSL cells were  
1493 mock-infected (lane 2), or infected with MCMVwt (lane 3) or MCMVwt UV-  
1494 inactivated (lane 4). Samples were lysed and processed as indicated in C. A lysate of  
1495 untransfected NIH3T3 cells (lane 1) was also subjected to western blot and employed as  
1496 a control. All infections were performed at an moi of 5 for 24 h. Data are representative  
1497 of at least two independent experiments. In C, E, and F, the size of the bands  
1498 corresponding to ICOSL are indicated on the right margin in kilodaltons (kDa). In E,  
1499 the sizes of the molecular weight markers are shown on the left side.

1500

1501 **Figure 5. m138 impedes ICOSL maturation redirecting it to lysosomal**  
1502 **degradation.** (A) Western blot analysis of NIH3T3 cells untransfected (lane 1) or  
1503 transiently co-transfected with either the HA-ICOSL and the control-GFP (CTL-GFP)  
1504 constructs (lanes 2 and 3), or the HA-ICOSL and the m138-GFP constructs (lanes 4 and  
1505 5) and, when indicated, treated with 250  $\mu$ M of leupeptin and 20 nM of bafilomycin A1  
1506 (lanes 3 and 5). The expression of ICOSL and actin was assessed as described in Figure  
1507 4C, and for the expression of the m138-GFP and CTL-GFP proteins a polyclonal  
1508 antibody anti-GFP followed by anti-rabbit IgG-HRP were used. (B) NIH3T3 HA-

1509 ICOSL were infected with MCMVwt at an moi of 5 for 24 h in the absence (-; panels a,  
1510 b, c and d) or presence of leupeptin and bafilomycin (panels e, f, g and h). Cells were  
1511 fixed, permeabilized, and stained with anti-m138 and anti-ICOSL mAbs followed by an  
1512 anti-mouse IgG-A555 and anti-rat IgG-A488, respectively. Nuclei were stained with the  
1513 DAPI reagent and samples were examined under a confocal fluorescence microscope.  
1514 Shown are representative cells from cultures stained for m138 (panels a, e), ICOSL (b,  
1515 f), and overlaid images (c, d, g, and h). Enlarged and more exposed individual cells  
1516 from panels c and g are presented on panels d and h, respectively. Magnification, x63.  
1517 (C) NIH3T3 HA-ICOSL infected and treated with the lysosomal inhibitors as in B were  
1518 fixed, permeabilized with the Foxp3 staining buffer set, and analyzed by flow cytometry  
1519 with anti-m138 and anti-ICOSL mAbs followed by an anti-mouse IgG-A555 and anti-  
1520 rat IgG-A488, respectively. Conditions were analyzed in triplicates and median  
1521 fluorescence intensity (MFI) values  $\pm$  SD were extracted from pre-gated m138  
1522 positive cells. (D) NIH3T3 cells were co-transfected with the m138-GFP and HA-  
1523 ICOSL constructs. HA-ICOSL was immunoprecipitated from 0.5% Triton treated  
1524 lysates using an anti-HA mAb or an anti-hFc as a control. Recovered  
1525 immunoprecipitates were subjected to SDS-PAGE and western blotting with antibodies  
1526 against GFP and HA, as described in A and Figure 4C. Data are representative of at  
1527 least two independent experiments. In A and D, the size of the two bands corresponding  
1528 to ICOSL, and in D, the band corresponding to m138-GFP, are indicated on the right  
1529 margin in kilodaltons (kDa). In A and D, the sizes of the molecular weight markers are  
1530 shown on the left side.

1531

1532 **Figure 6. Identification of the m138 domains involved in the downmodulation of**  
1533 **ICOSL and CD80.** (A) Schematic representation (not drawn to scale) of m138-GFP

1534 protein mutants. NIH3T3 ICOSL-HA cells were untransfected or transfected with  
1535 m138-GFP, or m138-GFP mutant constructs and analyzed by flow cytometry for  
1536 ICOSL and CD80 surface levels. Panels on the right represent the MFI of each sample  
1537 minus the MFI of the control isotypes. Grey histograms represent the expression of  
1538 untransfected cells and colored histograms represent the expression of cells transfected  
1539 with m138-GFP (green), m138 $\Delta$ Ig1-GFP (brown), m138 $\Delta$ Ig2-GFP (blue), or  
1540 m138 $\Delta$ Ig2/3-GFP (red). The isotype for each antibody was used as a negative control  
1541 (dotted lines). A representative experiment out of two performed is shown.

1542

1543 **Figure 7. m138 is capable to restrict CD8<sup>+</sup> T-cell activation by downregulating**  
1544 **ICOSL on the surface of APCs.** (A) C57BL/6 derived BMDCs were mock-infected or  
1545 infected for 24 hours with MCMVwt or MCMVm138 mutants at an moi of 3 and  
1546 analyzed by flow cytometry for surface expression of ICOSL and CD80 using specific  
1547 mAbs against each of these molecules. Grey histograms represent the expression of  
1548 mock-infected cells and colored histograms represent the expression of cells infected  
1549 (positive for the MCMV m04 protein) with MCMVwt (yellow), MCMV $\Delta$ m138 (pink),  
1550 MCMVm138 $\Delta$ Ig2 (blue), or MCMVm138 $\Delta$ Ig2/3 (red). The isotype for each antibody  
1551 was used as a negative control (black line histograms). Panels on the right represent the  
1552 MFI of each sample minus the MFI of the control isotypes. Results are representative of  
1553 two independent experiments (B) On the left, schematic representation of the *in vitro*  
1554 antigen-presentation assay. BMDCs infected as indicated in A with MCMVwt (yellow),  
1555 MCMV $\Delta$ m138 (pink), MCMVm138 $\Delta$ Ig2 (blue), or MCMVm138 $\Delta$ Ig2/3 (red), or left  
1556 uninfected (grey) were further co-cultured with naïve CD8<sup>+</sup> T cells from Maxi mice.  
1557 After 6 h, IFN- $\gamma$  production by CD8<sup>+</sup> T cells was determined by flow cytometry. Results

1558 are representative of three independent experiments. Results are expressed as the mean  
1559 +/-SEM of the percentage values obtained for samples in each group.

1560

1561 **Figure 8. Via targeting ICOSL, m138 reduces T-cell mediated control of MCMV**

1562 **infection *in vivo*.** (A) BALB/c mice were intraperitoneally (i.p.) inoculated with  $2 \times 10^6$

1563 PFU MCMV-GFP. 2 days post infection mice were sacrificed and peritoneal exudate

1564 cells were extracted and analyzed by flow cytometry for surface expression of ICOSL

1565 and MHCI, using specific mAbs against each of these molecules. Blue histograms

1566 represent the expression of uninfected (GFP-) cells and green histograms represent the

1567 expression of MCMV-infected (GFP+) cells from the same mouse. The isotype for each

1568 antibody was used as a negative control (dotted lines). The results obtained from a

1569 representative infected mouse out of two are shown. (B) BALB/c mice (n=4/group)

1570 were mock-infected or i.p. infected with  $1 \times 10^6$  PFU of MCMVwt or MCMV $\Delta$ m138. At

1571 six hpi, peritoneal exudate cells were extracted and surface expression of ICOSL and

1572 CD80 assessed by flow cytometry on the surface of DCs (CD11<sup>+</sup> MHC II<sup>+</sup> CD3<sup>-</sup>CD19<sup>-</sup>

1573 NKp46<sup>-</sup> cells), gating on m04 positive cells when derived from MCMVwt- or

1574 MCMV $\Delta$ m138-infected mice. Results are expressed as the mean +/-SD of the MFI

1575 values obtained for samples from two independent experiments. (C) Table displaying

1576 the immunomodulatory effects of the different MCMVs on the cellular targets of m138.

1577 (D) On the top, a schematic representation of the MCMV $\Delta$ m138 and MCMVm138 $\Delta$ Ig2

1578 *in vivo* infection assay is shown. C57BL/6 mice (n=5-7/group) with or without NK, or

1579 NK, CD4<sup>+</sup> and CD8<sup>+</sup> T-cell depletion, as indicated, were intravenously (i.v.) inoculated

1580 with  $2 \times 10^5$  PFU/mouse of MCMVwt (yellow circles), MCMV $\Delta$ m138 (pink triangles) or

1581 MCMVm138 $\Delta$ Ig2 (blue triangles). At day 14 post infection mice were sacrificed and

1582 viral titers in salivary glands and lungs of individual mice were determined by standard



1583 plaque assays. Horizontal bars indicate the median values. The Kruskal-Wallis test was  
1584 used to assess statistical differences between experimental groups. \* $p < 0.05$ , \*\* $p < 0.01$ .  
1585 A representative experiment out of two performed is shown.  
1586 The online version of this article includes the following figure supplements for figure 8:  
1587 Figure supplement 1. **m138 contributes to immune evasion of D4<sup>+</sup> T cells in spleens**  
1588 **and lungs of MCMV infected mice.**  
1589  
1590 **Figure 9. Blockade of ICOSL reduces the frequency of particular lymphocyte**  
1591 **subsets in the spleen and lymph nodes of MCMV infected mice.** (A) BALB/c mice  
1592 (n=11-12/group) were i.p. inoculated with  $2 \times 10^6$  PFU of MCMV $\Delta$ m138 and treated  
1593 with ( $\alpha$ -ICOSL) or without (CTL) 100 mg of anti-ICOSL mAb. At day 14 post  
1594 infection mice were sacrificed, and spleens and lymph nodes were isolated and  
1595 disaggregated. Cell suspensions were analyzed by flow cytometry using anti-mouse  
1596 CD3, CD4, CD8, CD44, CD62L, CXCR5 and PD1 for T-cell phenotype. For B cell  
1597 phenotype B220, CD21, CD23, CD95 and GL7 mAbs were used. Percentages of Tfh  
1598 cells (CD3<sup>+</sup>CD4<sup>+</sup>CXCR5<sup>hi</sup>PD1<sup>hi</sup>), germinal center (GC) B cells (CD95<sup>hi</sup>GL7<sup>hi</sup>B220<sup>+</sup>),  
1599 follicular (FO) B cells (CD21<sup>+</sup>CD23<sup>+</sup>B220<sup>+</sup>), and CD3<sup>+</sup>CD4<sup>+</sup> or CD3<sup>+</sup>CD8<sup>+</sup> naïve  
1600 (CD44<sup>low</sup>CD62L<sup>hi</sup>) and memory (CD44<sup>hi</sup>CD62L<sup>low</sup>) T cells from these two organs are  
1601 shown. (B) Representative immunofluorescence of spleens from mice infected and  
1602 treated with (panels b and d) or without (panels a and c) the anti-ICOSL mAb, as  
1603 indicated in A. Two color colocalization with B220 in green and peanut agglutinin  
1604 (PNA) in red are shown at x4 and x10 magnifications. Panels on the right show a  
1605 graphic representation of follicle and germinal center relative areas from tissue sections  
1606 of a representative mouse of each experimental group. In graphs shown in A and B,  
1607 results are expressed as mean +/- SD. Mice treated with anti-ICOSL mAb are

1608 represented as red squares and mice not receiving the mAb are represented as open  
1609 circles. Two-tailed unpaired *t*-tests were used to assess statistical differences between  
1610 experimental groups. \**p*<0.05, \*\**p*<0.01, \*\*\**p*<0.001, \*\*\*\**p*<0.0001. Data are pooled  
1611 from two independent experiments.

1612 The online version of this article includes the following figure supplements for figure 9:  
1613 Figure supplement 1. **Effect of ICOSL blockade on the frequency of several**  
1614 **lymphocyte subsets in the spleen and lymph nodes of MCMV infected mice.**

1615

1616 **Figure 10. ICOSL blockade limits the generation of MCMV specific antibodies.** (A)  
1617 Total levels of IgG, IgG1, IgG2a, IgG2b, IgG3 (at dilutions 1:200 and 1:400), and IgM  
1618 (at dilutions 1:25 and 1:50) were determined by ELISA from sera collected at day 14 of  
1619 the same infected BALB/c mice indicated in Figure 8A. (B) Sera (at dilutions 1:10 and  
1620 1:100) as in A were tested in a viral neutralization assay. Results are presented as the  
1621 percentage of plaque reduction determined by the ratio of the number of plaques  
1622 counted in the sample wells relative to the ratio of plaques in wells containing the serum  
1623 of an uninfected mouse used as a negative control. In A and B, results are expressed as  
1624 mean +/- SD. Mice treated with anti-ICOSL mAb are represented as red squares and  
1625 mice that did not receive the mAb are represented as open circles. Two-tailed unpaired  
1626 *t*-tests were used to assess statistical differences between experimental groups. \**p*<0.05,  
1627 \*\**p*<0.01, \*\*\**p*<0.001. Data are pooled from two independent experiments.

1628 The online version of this article includes the following figure supplements for figure  
1629 10:

1630 Figure supplement 1. **Effect of ICOSL blockade on MCMV neutralization in the**  
1631 **presence of complement.**

1632

1633 **Figure 11. HCMV, HSV-1, and HSV-2 also limit cell surface expression of ICOSL**  
1634 **on APCs.** (A) Primary monocyte-derived macrophages (upper panels) and PMA-treated  
1635 THP-1 cells (bottom panels) were mock-infected or infected for 72 hours with HCMV-  
1636 GFP at an moi of 10 and analyzed by flow cytometry for cell-surface expression of  
1637 human ICOSL or CD70 using specific mAbs against each of these receptors. Gray  
1638 histograms represent the expression of mock-infected cells, green histograms represent  
1639 the expression on HCMV-infected (GFP+) cells, and blue histograms represent the  
1640 expression on uninfected (GFP-) cells from the same culture. (B) PMA-treated THP-1  
1641 cells were mock-infected (time 0) or infected with HCMV-GFP as in A and analyzed by  
1642 flow cytometry for surface expression of ICOSL at the different time points after  
1643 infection indicated. (C) Same as in A, except that an moi of 20 was used, and THP-1  
1644 cells were also exposed for 72 h to the same amount of HCMV-GFP UV-inactivated  
1645 (red histogram). (D) Equal amounts of lysates from PMA-treated THP-1 cells mock-  
1646 infected (lane 1) or infected for 72 h at an moi of 20 with HCMV-GFP (lanes 2 and 3),  
1647 and when indicated, treated with 250  $\mu$ M leupeptin and 20 nM of bafilomycin A1 (lane  
1648 3), were lysed and analyzed by western blot with antibodies against ICOSL and actin,  
1649 followed by anti-rabbit IgG-HRP (ICOSL) or anti-mouse IgG-HRP (actin). (E) PMA-  
1650 treated THP-1 cells were mock-infected or infected with HSV-1-GFP, HSV-1-GFP UV-  
1651 inactivated, HSV-2-GFP or HSV-2-GFP UV-inactivated at an moi of 100 (HSV-1) or  
1652 200 (HSV-2). 24 h later the expression of human ICOSL and CD70 were analyzed as in  
1653 A. Green histograms represent the expression of ICOSL on infected cells, red  
1654 histograms represent the expression on UV-inactivated HSV infected cells, and grey  
1655 histograms represent the expression on mock-infected cells. The isotype for the ICOSL  
1656 antibody was used as a negative control (dotted lines). A representative experiment out  
1657 of three performed is shown. (F) PMA-treated THP-1 cells were mock-infected (lane 1)

1658 or infected with HSV-1-GFP (lane 2) and HSV-2-GFP (lane 3) as indicated in E. Cell  
1659 lysates were prepared, and subjected to western blot analysis using an anti-human  
1660 ICOSL or anti-actin mAbs as in D. The molecular weight of the band corresponding to  
1661 ICOSL is indicated in D and E in kilodaltons on the right margin.

1662

1663 **Figure 3-figure supplement 1. Localization of m138 in MCMV-infected DC2.4**  
1664 **cells.** D2.4 cells were infected with MCMV-GFP at an moi of 5 for 24 h, fixed with 4%  
1665 formaldehyde, permeabilized with 0.05% Triton, and stained with the anti-m138 mAb  
1666 followed by an anti-mouse IgG-A555. Nuclei were stained with the DAPI reagent. The  
1667 cells were examined under a fluorescence microscope. Magnification, x20 (a-c); an  
1668 enlarged individual cell from panel c is shown in panel d.

1669

1670 **Figure 8-figure supplement 1. m138 contributes to immune evasion of D4<sup>+</sup> T cells**  
1671 **in spleens and lungs of MCMV infected mice.** On the top, a schematic representation  
1672 of the adoptive transfer *in vivo* assay is shown.  $1 \times 10^5$  M25-specific transgenic CD4<sup>+</sup> T  
1673 cells were transferred (i.v.) into C57BL/6 SCID mice (n=4-5/group), which were  
1674 depleted of NK cells as indicated, and either mock-infected or i.p. infected with  $2 \times 10^5$   
1675 PFU/mouse of MCMVwt or MCMV $\Delta$ m138. Seven dpi, spleens, lungs and salivary  
1676 glands were harvested, and analyzed by flow cytometry using anti-CD45.1 and anti-  
1677 CD4 specific mAbs. The frequency of CD45.1<sup>+</sup> CD4<sup>+</sup> cells for each organ is indicated.  
1678 Results are expressed as the mean +/-SEM of the percentage values obtained for  
1679 samples in each group.

1680

1681 **Figure 9-figure supplement 1. Effect of ICOSL blockade on the frequency of**  
1682 **several lymphocyte subsets in the spleen and lymph nodes of MCMV infected mice.**

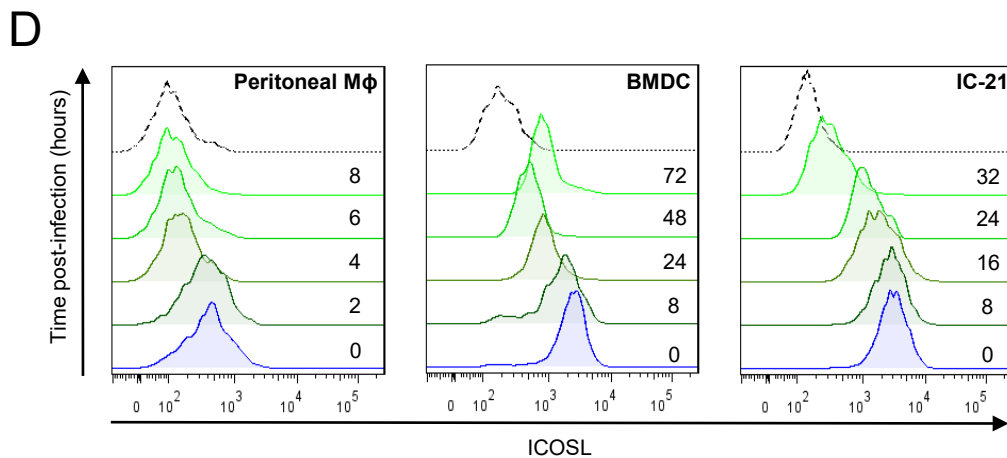
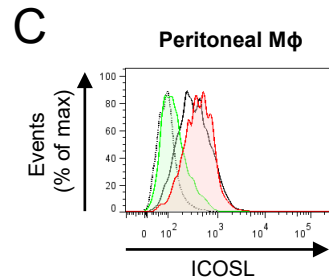
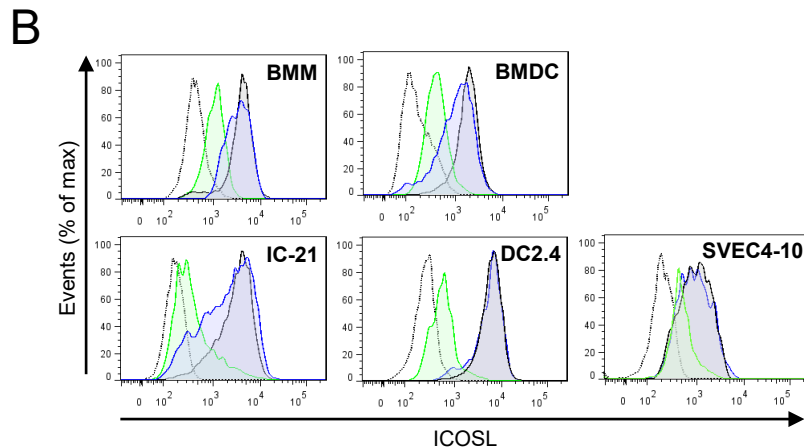
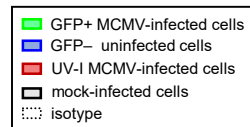
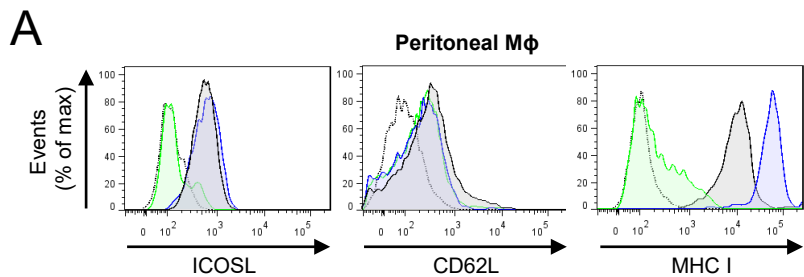
1683 Cell suspensions obtained from spleens and lymph nodes of BALB/c mice infected and  
1684 treated as indicated in Figure 8A were analyzed by flow cytometry using anti-mouse  
1685 CD3, CD4, CD8, CD5, B220, CD23, CD21, CD138, and CD19 mAbs, and anti-mouse  
1686 IgM polyclonal Ab. Percentages of total B cells (B220<sup>+</sup>), marginal zone (MZ) B cells  
1687 (CD21<sup>+</sup>CD23<sup>-</sup>B220<sup>+</sup>), B1 B cells (CD19<sup>hi</sup>B220<sup>int</sup>), B1a (CD19<sup>hi</sup>B220<sup>int</sup>CD5<sup>+</sup>) and B1b  
1688 (CD19<sup>hi</sup>B220<sup>int</sup>CD5<sup>-</sup>) subsets, CD3<sup>+</sup>CD4<sup>+</sup> or CD3<sup>+</sup>CD8<sup>+</sup> T cells, and plasma cells  
1689 (CD138<sup>hi</sup>B220<sup>low</sup>CD19<sup>-</sup>IgM<sup>+</sup>) are shown. Results are expressed as mean +/- SD. Mice  
1690 treated with anti-ICOSL mAb are represented as red squares and mice untreated are  
1691 represented as open circles. Two-tailed unpaired *t*-test was used to assess statistical  
1692 differences between experimental groups.

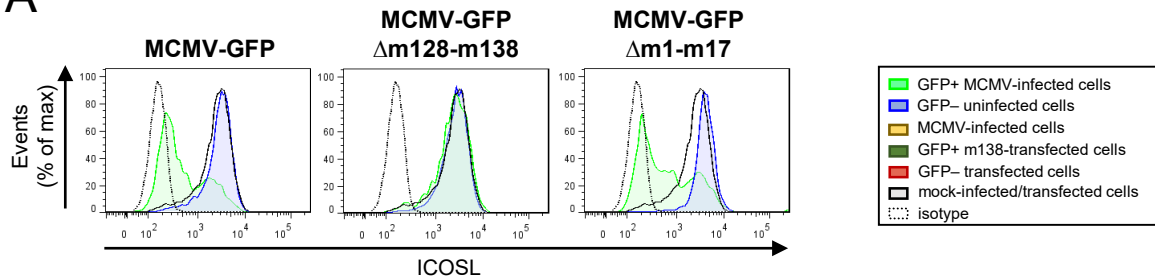
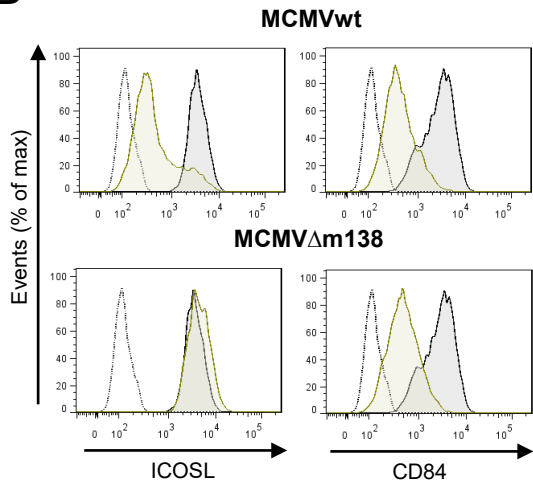
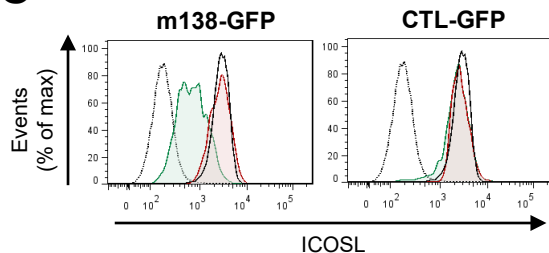
1693

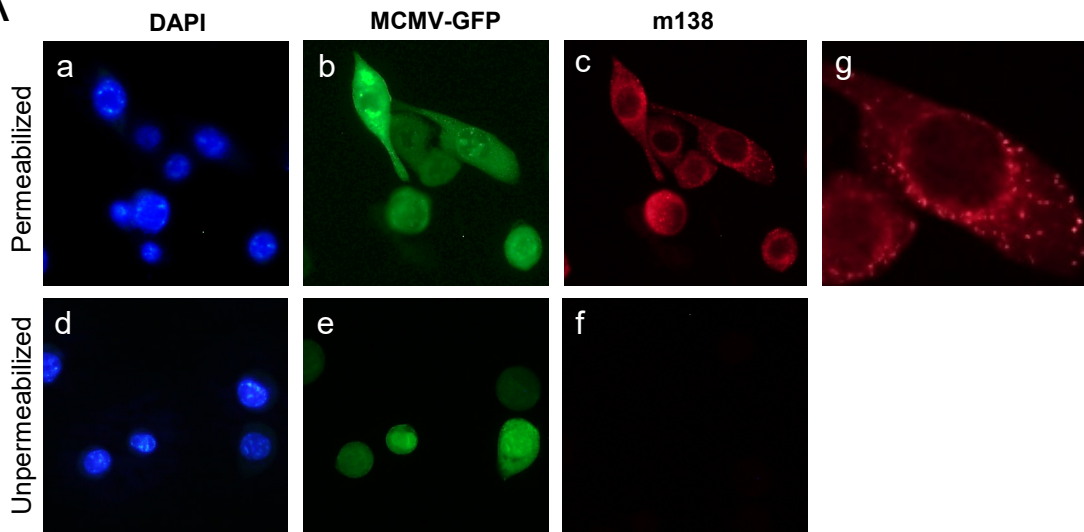
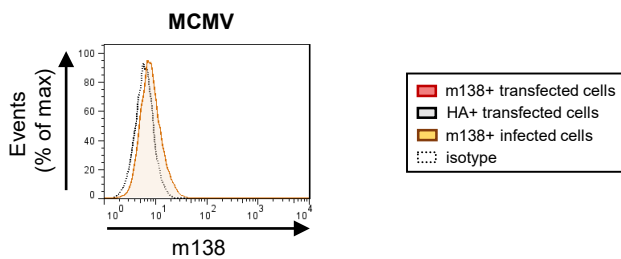
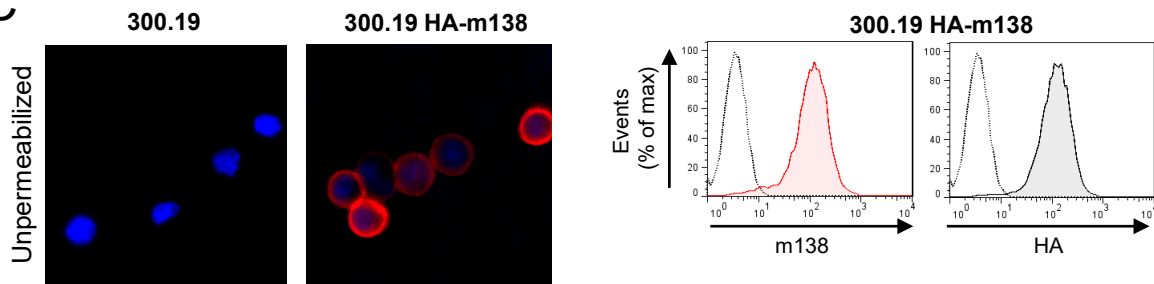
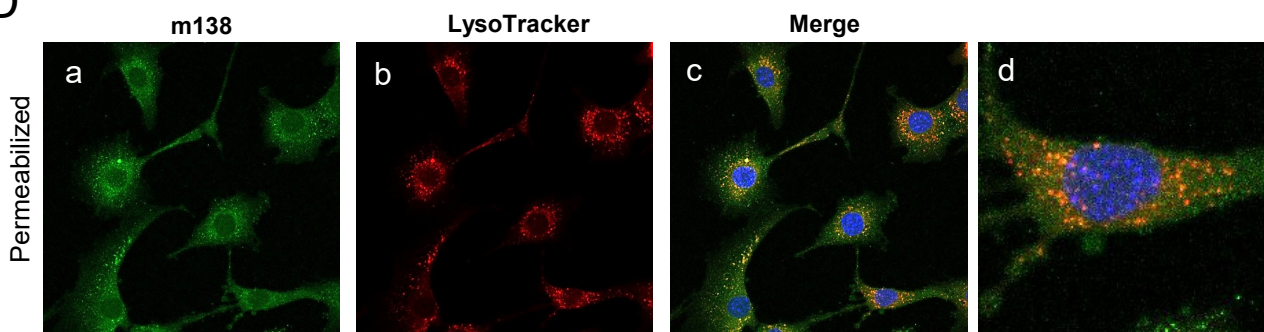
1694 **Figure 10-figure supplement 1. Effect of ICOSL blockade on MCMV**  
1695 **neutralization in the presence of complement.** Same as in Figure 9B, except that the  
1696 MCMV neutralization assay was performed in the presence of rabbit complement.  
1697 Results are presented as the percentage of plaque reduction determined by the ratio of  
1698 the number of plaques counted in the sample wells relative to the ratio of plaques in  
1699 wells containing the serum of an uninfected mouse used as a negative control. Results  
1700 are expressed as mean +/- SD. Mice treated with anti-ICOSL mAb are represented as  
1701 red squares and mice untreated are represented as empty circles. Two-tailed unpaired *t*-  
1702 test was used to assess statistical differences between experimental groups. \**p*<0.05,  
1703 \*\**p*<0.01.

1704

1705 **Supplementary File 1. Key Resources Table.**



**A****B****C**

**A****B****C****D**

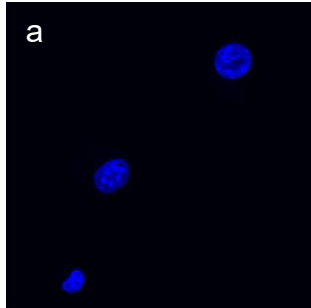


DAPI

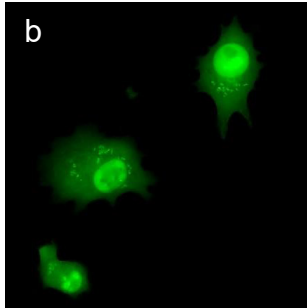
MCMV-GFP

m138

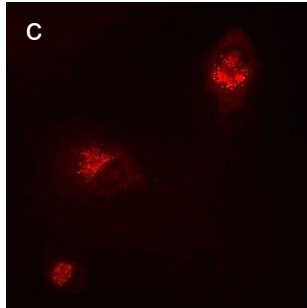
a



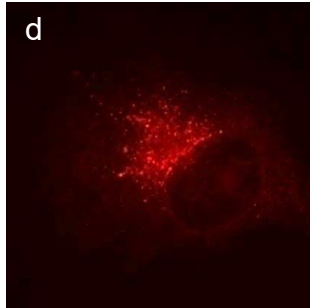
b

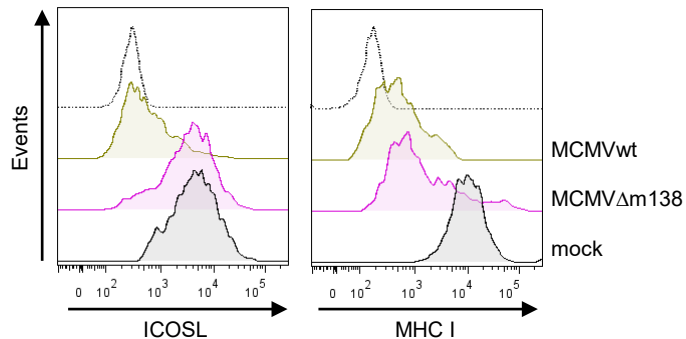
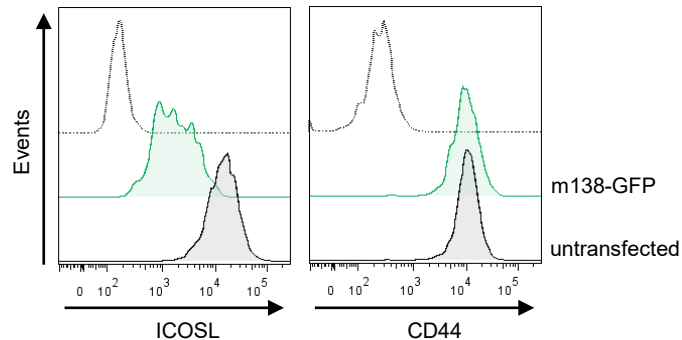
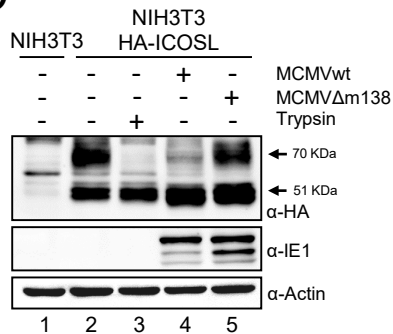
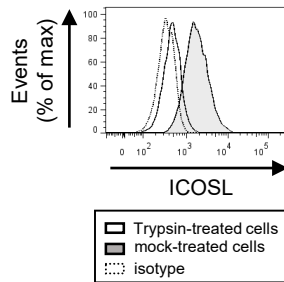
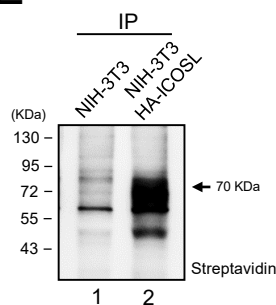
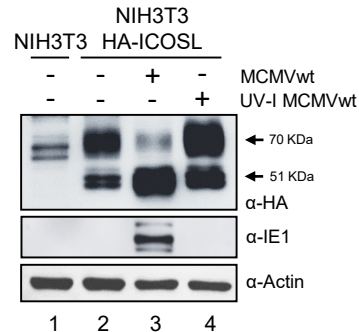


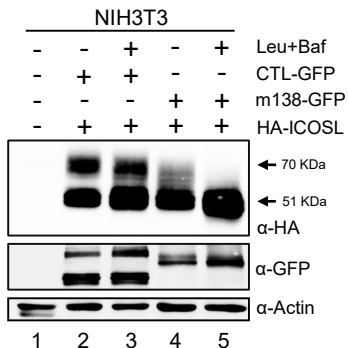
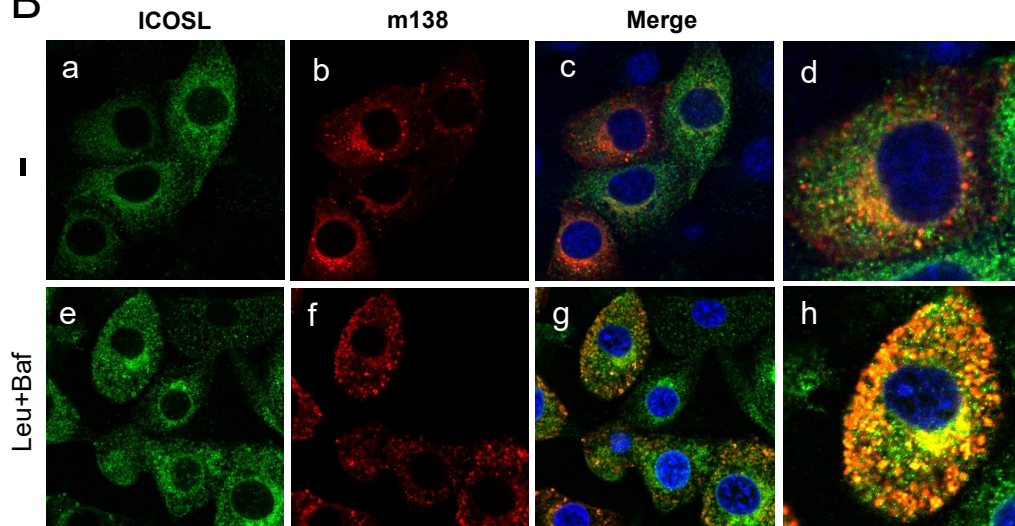
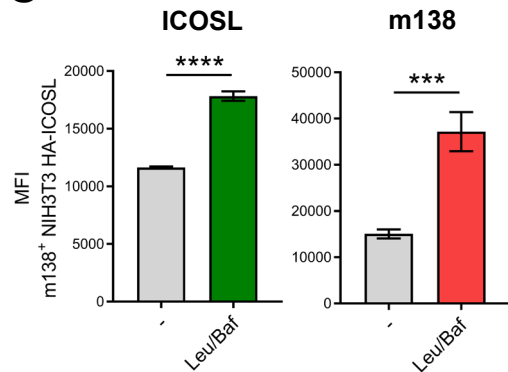
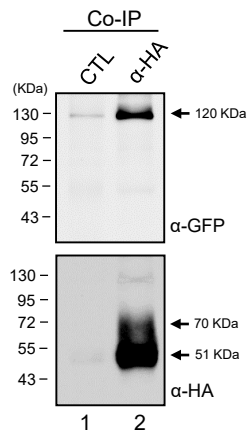
c



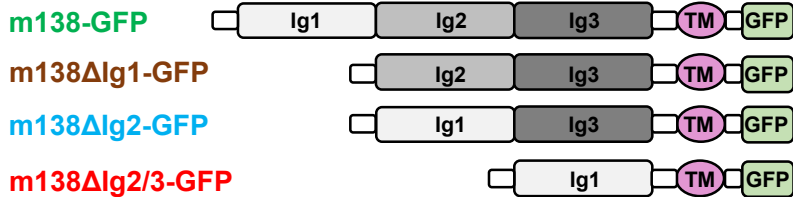
d



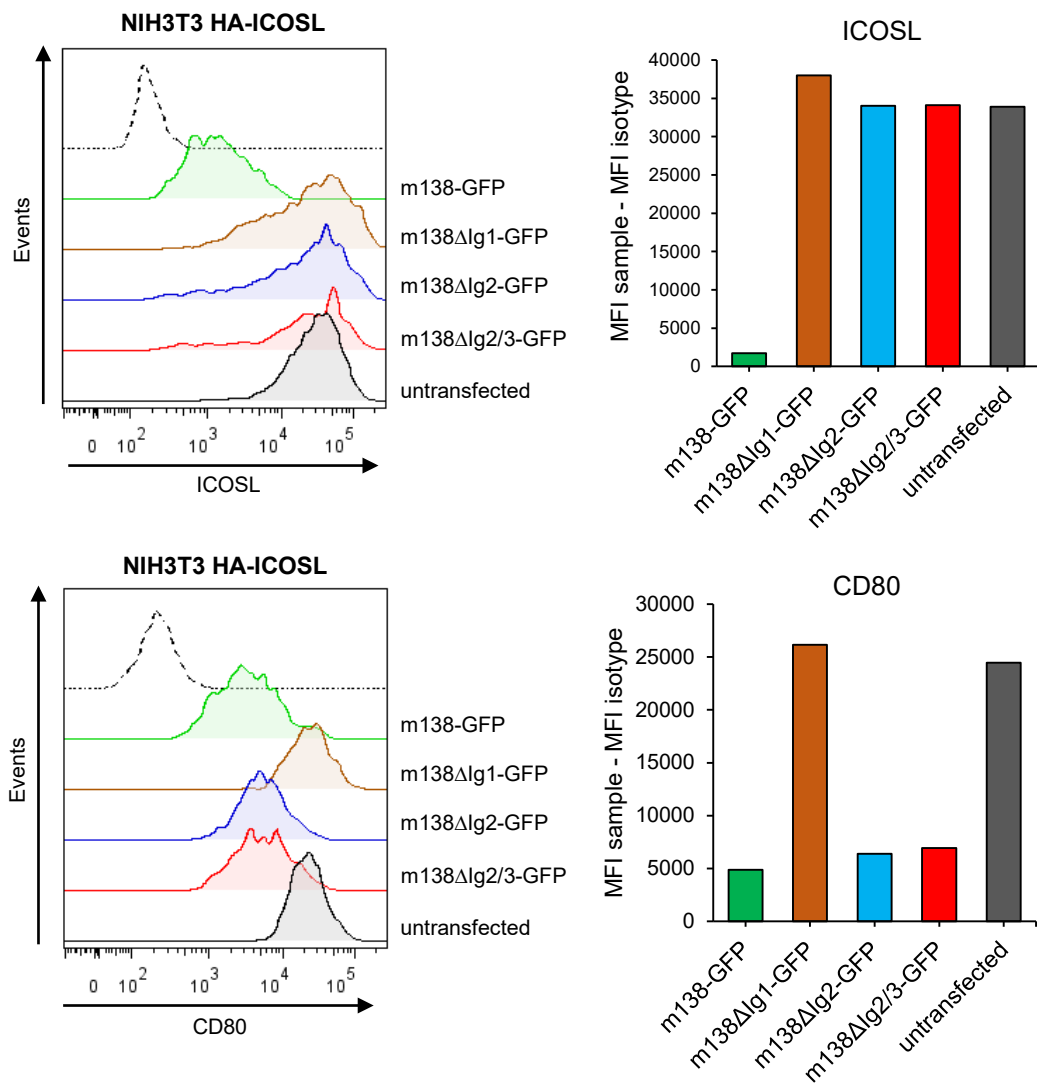
**A****NIH3T3 HA-ICOSL****B****NIH3T3 HA-ICOSL****C****D****E****F**

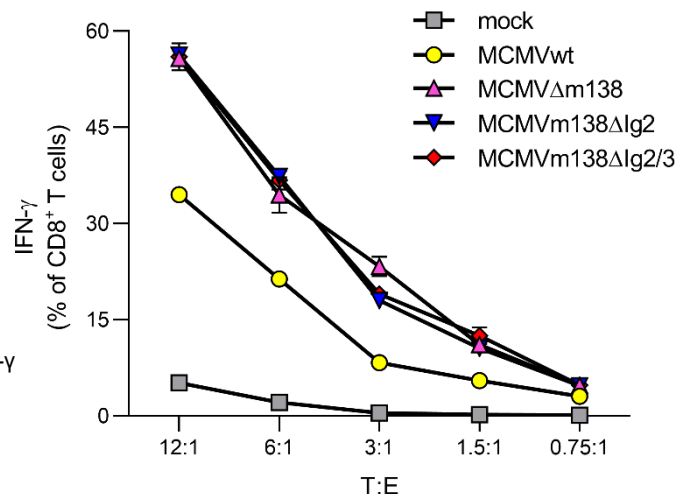
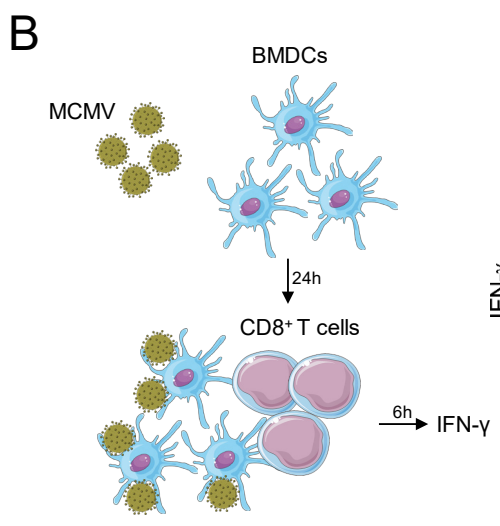
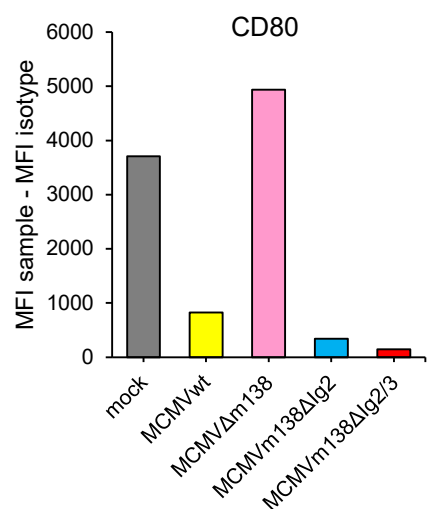
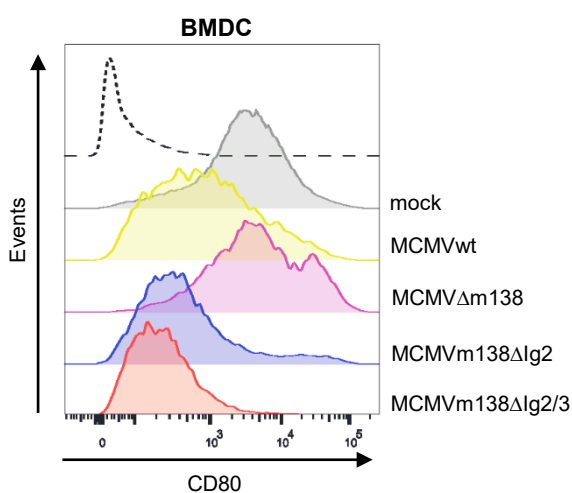
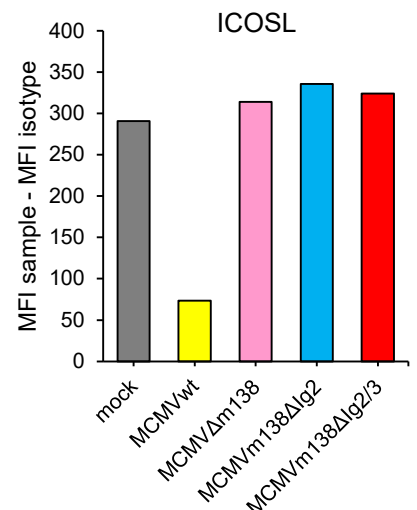
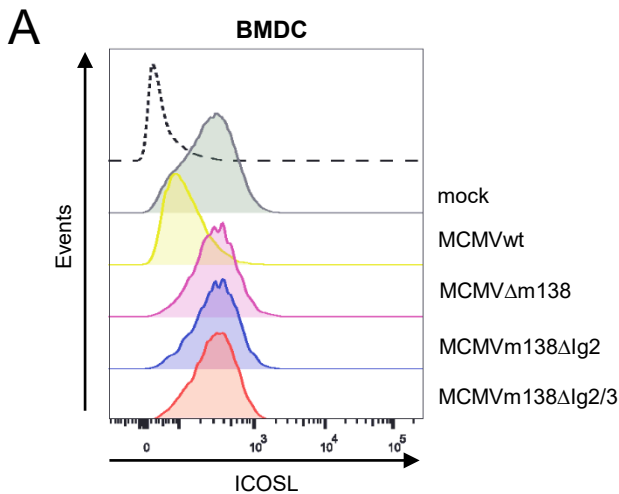
**A****B****C****D**

A

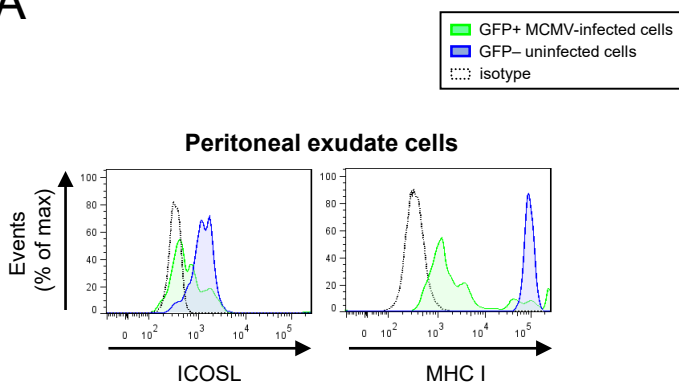


B

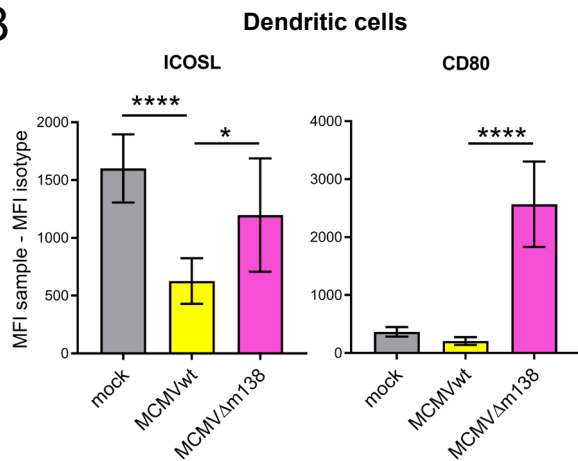




A



B

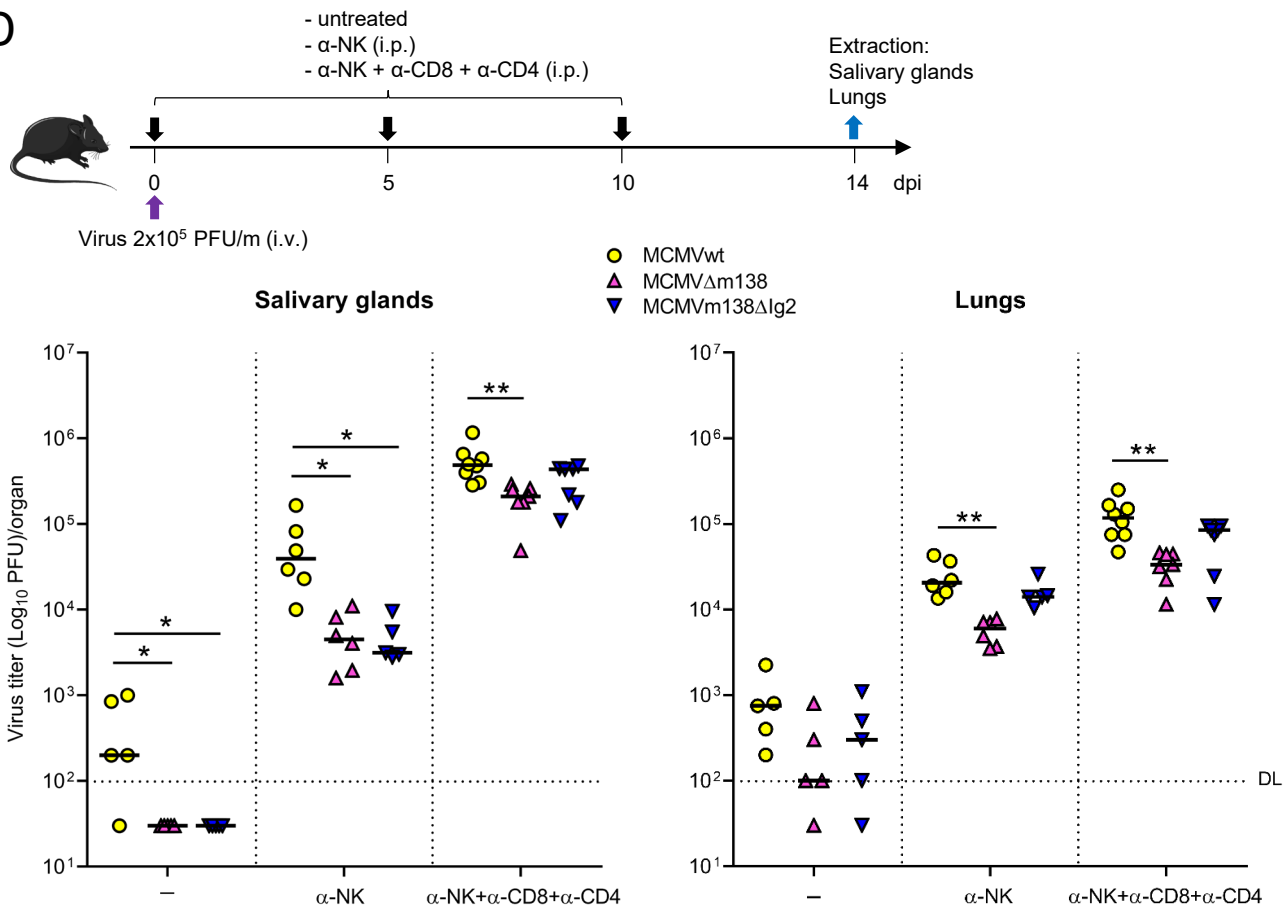


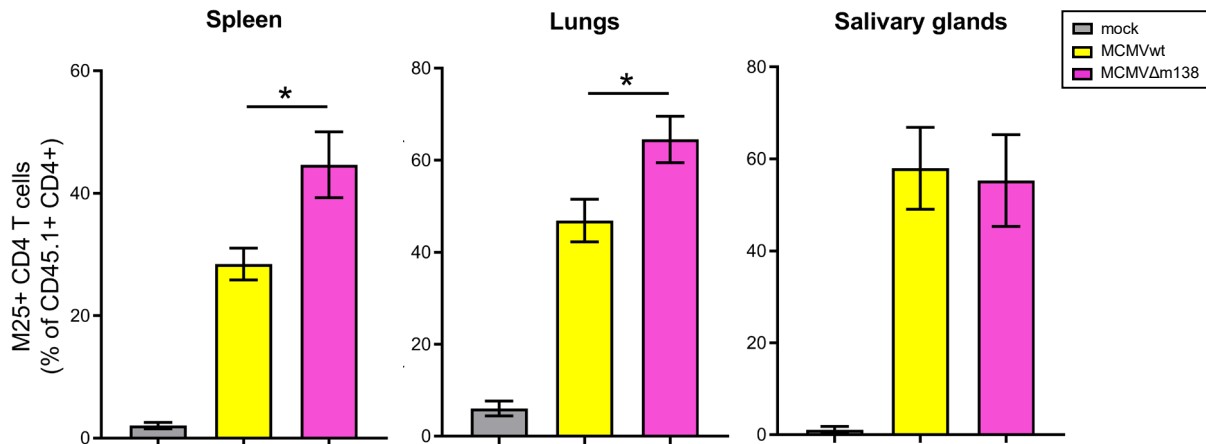
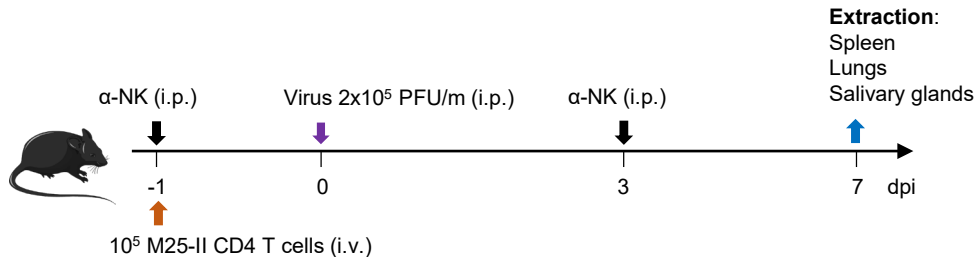
C

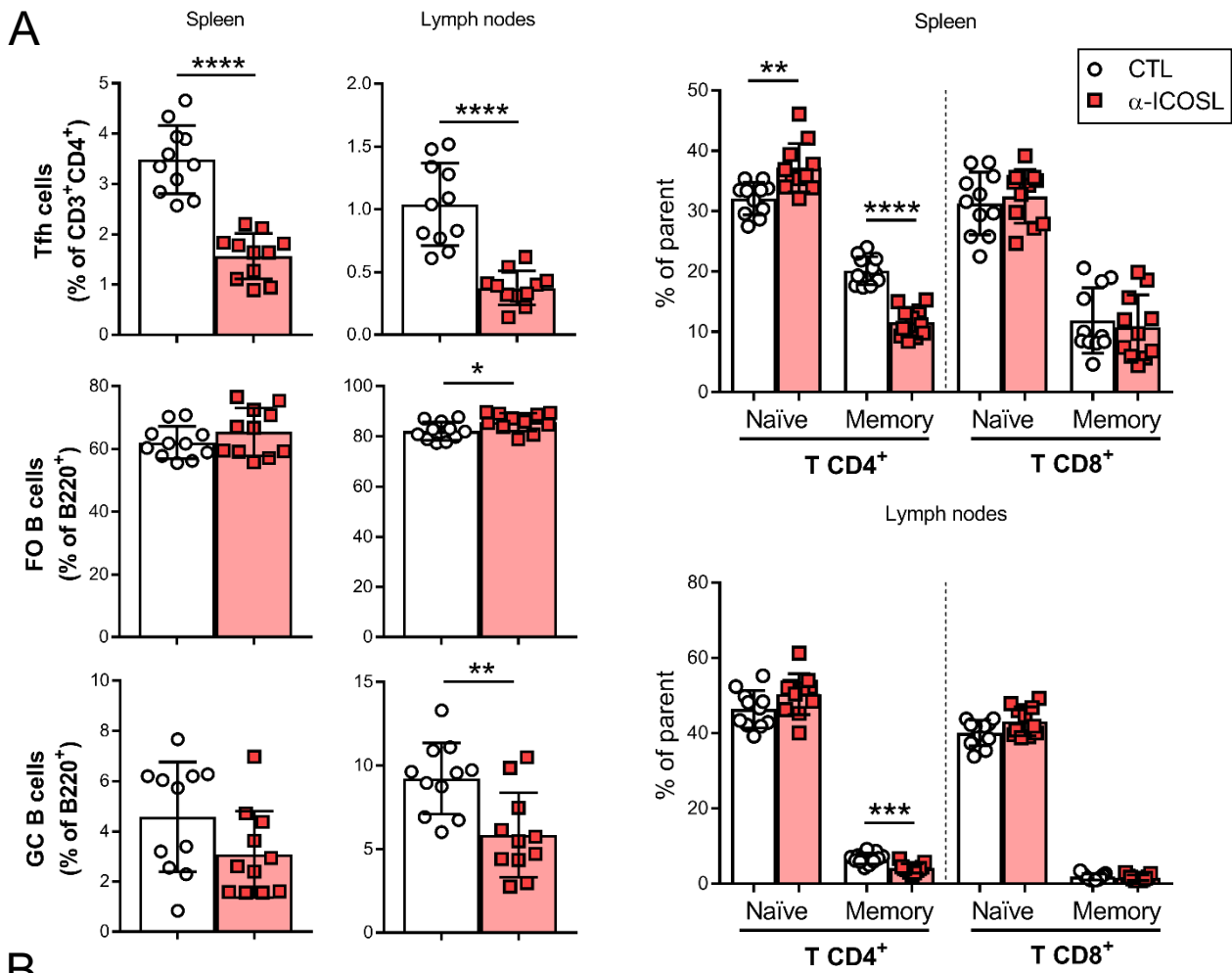
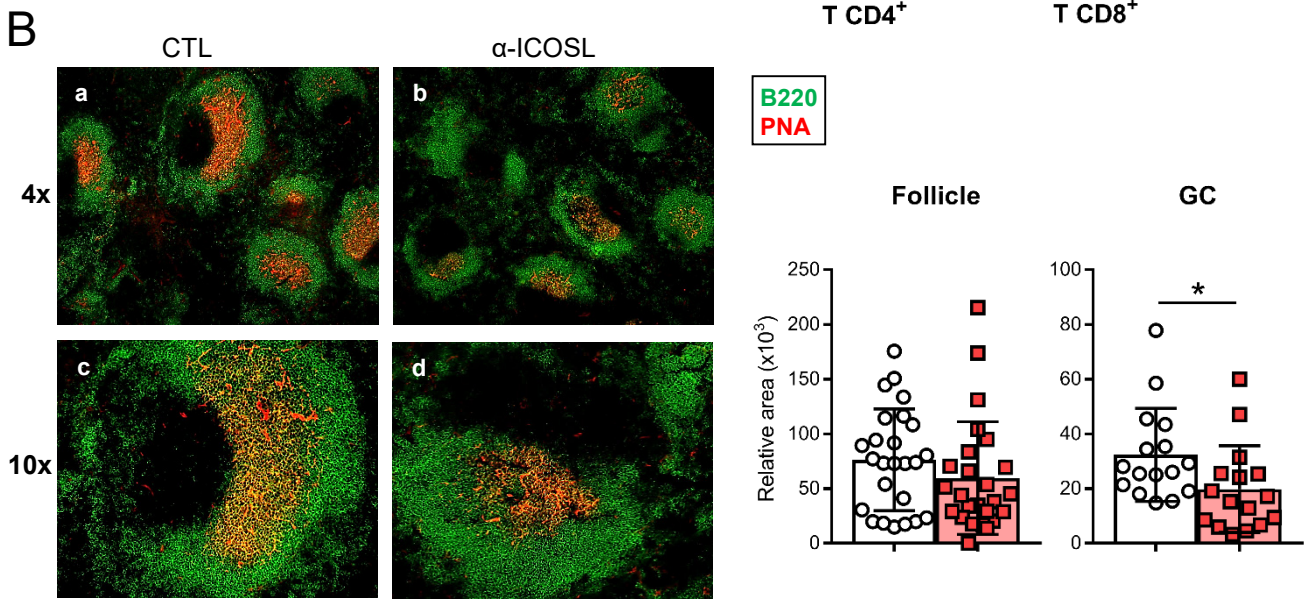
Viruses	NKG2D ligands			co-stimulatory molecules	
	MULT-1	RAE-I $\epsilon$	H60	ICOSL	CD80
MCMVwt (full length m138)	downregulated	downregulated	downregulated	downregulated	downregulated
MCMV $\Delta$ m138 (m138 deleted)	not altered	not altered	not altered	not altered	not altered
MCMVm138 $\Delta$ lg2 (m138 lg2 domain deleted)	downregulated	downregulated	not altered	not altered	downregulated

Effects of MCMVwt and mutants on m138 targets at the surface of infected cells

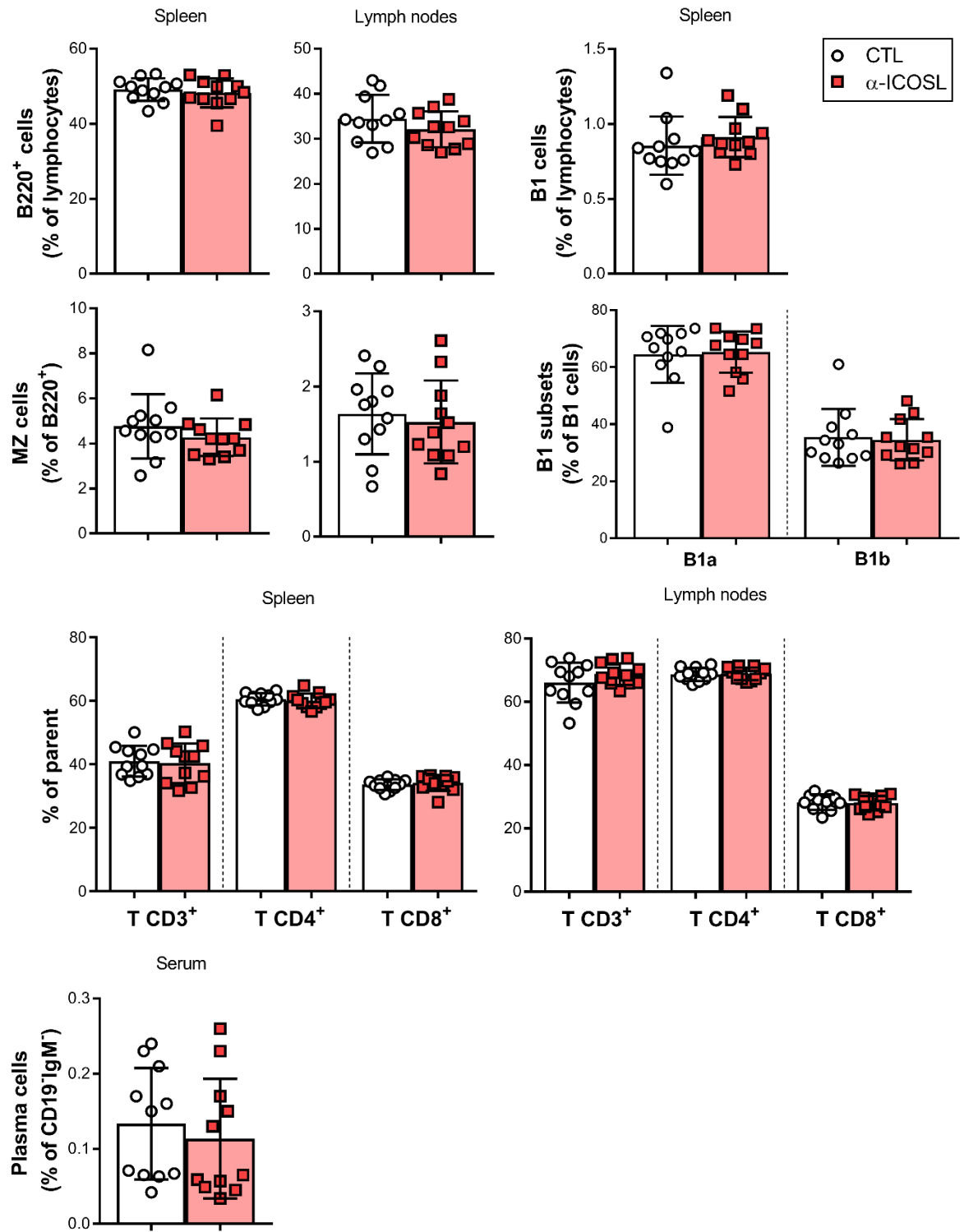
D

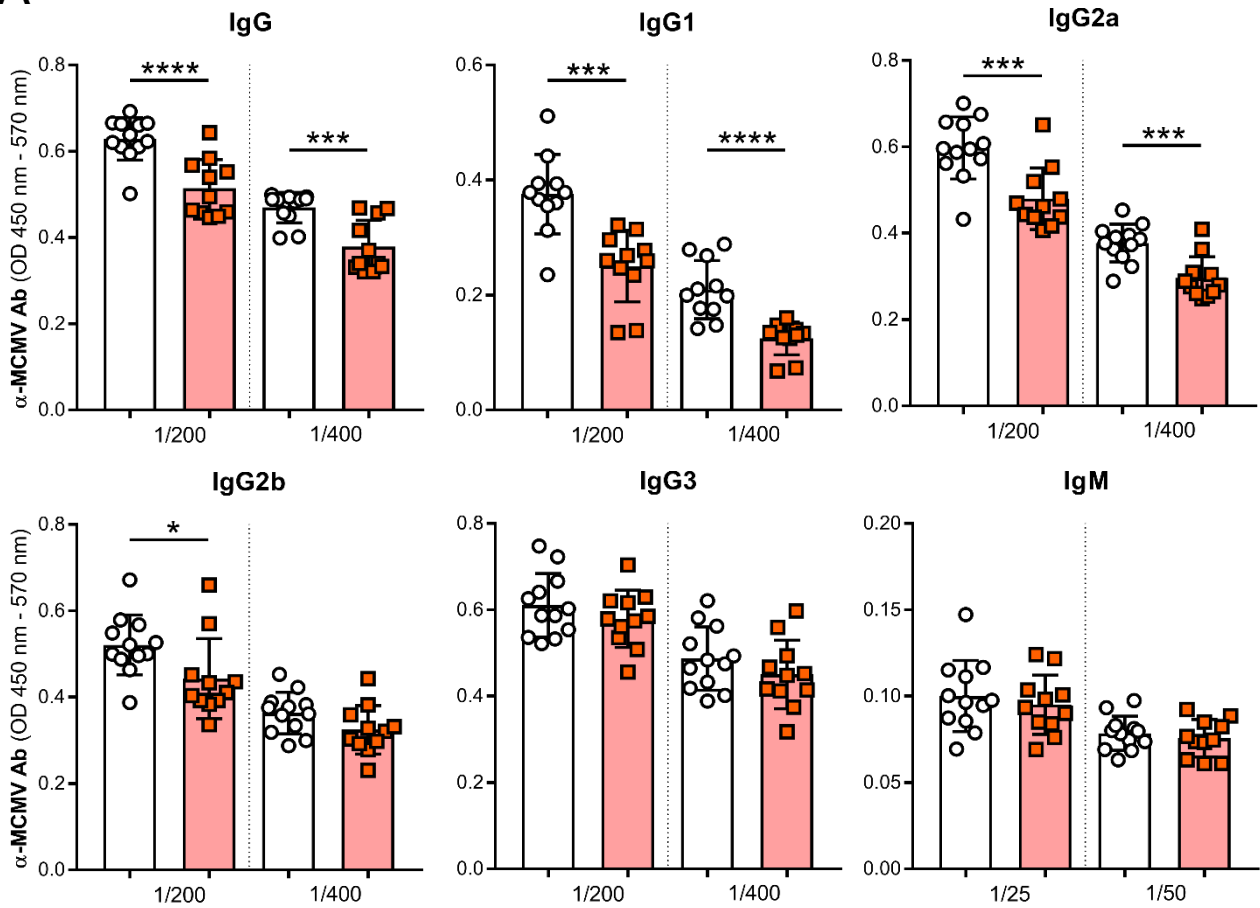




**A****B**





**A****B**